eNeuro

Research Article: New Research | Disorders of the Nervous System

Neuregulin 1 Type-I over-Expression Is Associated with Reduced NMDA Receptor-Mediated Synaptic Signaling in Hippocampal Interneurons Expressing PV or CCK

D. Kotzadimitriou[1], W. Nissen[1], M. Paizs[2], K. Newton[1], P. J. Harrison[3], O. Paulsen[4] and K. Lamsa[1,2]

[1]*Department of Pharmacology, University of Oxford, Mansfield Road, Oxford, OX1 3QT, UK*

[2]*Department of Physiology, Anatomy and Neuroscience, University of Szeged, Közép Fasor 52, Szeged, 6720, Hungary*

[3]*Department of Psychiatry, University of Oxford, and Oxford Health NHS Foundation Trust, Oxford, UK*

[4]*Department of Physiology, Development and Neuroscience, University of Cambridge, Cambridge, UK*

DOI: 10.1523/ENEURO.0418-17.2018

Received: 4 December 2017

Revised: 25 February 2018

Accepted: 28 February 2018

Published: 20 April 2018

Author Contributions: Designed research (PJH, DK, KL, WN, OP), Performed research (DK, KL, KN, WN, MP). Contributed unpublished reagents/ analytic tools (N/A), Analyzed data (DK, WN, MP, KN, KL), Wrote the paper (DK, KL, WN).

Funding: The Medical Research Council UK; the John Fell OUP Research Fund; Wellcome Trust UK; Hungarian Academy of Sciences Neuroscience Program; Oxford University Vice-Chancellor's Grant; The Biotechnology and Biological Sciences Research Council UK;

Conflict of Interest: Authors report no conflict of interest.

This work was supported by the Medical Research Council UK (DK, KL, KN, WN, OP), the John Fell OUP Research Fund (KL), the Biotechnology and Biological Sciences Research Council UK (OP), Wellcome Trust (PJH, KL), Hungarian Academy of Sciences Neuroscience Program 2017-1.2.1-NKP-2017-00002 (KL, MP), and the Oxford University Vice-Chancellor's grant (WN).

D.K. and W.N. equal contribution.

Correspondence: Karri Lamsa, Department of Physiology, Anatomy and Neuroscience, University of Szeged, Kozep fasor 52, 6720 Szeged, Hungary. Email: klamsa@bio.u-szeged.hu

Cite as: eNeuro 2018; 10.1523/ENEURO.0418-17.2018

Manuscript Title Page

1. Manuscript Title: **Neuregulin 1 type-I over-expression is associated with reduced NMDA receptor-mediated synaptic signaling in hippocampal interneurons expressing PV or CCK**

2. Abbreviated Title: *NMDAR hypofunction in interneurons by NRG1 type-I*

3. List all Author Names and Affiliations in order as they would appear in the published article: Kotzadimitriou D.[1#], Nissen W.[1#], Paizs, M.[2], Newton K.[1], Harrison P.J.[3], Paulsen O.[4], Lamsa K.[1,2]*

[1]Department of Pharmacology, University of Oxford, Mansfield Road, OX1 3QT Oxford, UK. [2]Department of Physiology, Anatomy and Neuroscience, University of Szeged, Közép fasor 52, 6720 Szeged, Hungary. [3]Department of Psychiatry, University of Oxford, and Oxford Health NHS Foundation Trust, Oxford, UK. [4]Department of Physiology, Development and Neuroscience, University of Cambridge, Cambridge, UK.

[#]equal contribution

4. Author Contributions: Designed research (PJH, DK, KL, WN, OP), Performed research (DK, KL, KN, WN, MP). Contributed unpublished reagents/ analytic tools (N/A), Analyzed data (DK, WN, MP, KN, KL), Wrote the paper (DK, KL, WN).

5. *Correspondence: Karri Lamsa, Department of Physiology, Anatomy and Neuroscience, University of Szeged, Kozep fasor 52, 6720 Szeged, Hungary.
Email: klamsa@bio.u-szeged.hu

6. Number of Figures: 6
7. Number of Tables: N/A
8. Number of Multimedia: N/A
9. Number of words for Abstract: 250
10. Number of words for Significance Statement: 120
11. Number of words for Introduction: 519
12. Number of words for Discussion: 1280

13. Acknowledgements: We thank Dr Ed Mann for donating Ai9 and Ai9xPV-Cre mice, Drs Klaus-Armin Nave and Markus Schwab (MPI Göttingen, Germany) for the gift of NRG1$^{tg\text{-}type\text{-}I}$ mice; Dr Andres Buonanno (National Institute of Child Health and Human Development, Bethesda, Maryland 20892, USA.) for the rabbit anti-ErbB4 antibody; Dr Andras Szabo for help in anatomical analysis and cell reconstructions, Linda Avena, Fabian Peters and Matt Prior for contributing to initial experiments; Drs Marco Bocchio, Alexei Bygrave, Marco Capogna and Liliana Minichiello, Pavel Perestenko and Ayesha Sengupta, for scientific advice and discussions, and the Peter Somogyi laboratory in MRC ANU for help with anatomical and immunohistochemical procedures.

14. Conflict of Interest: Authors report no conflict of interest.

15. Funding sources: This work was supported by the Medical Research Council UK (DK, KL, KN, WN, OP), the John Fell OUP Research Fund (KL), the Biotechnology and Biological Sciences Research Council UK (OP), Wellcome Trust (PJH, KL), Hungarian Academy of Sciences Neuroscience Program 2017-1.2.1-NKP-2017-00002 (KL, MP), and the Oxford University Vice-Chancellor's grant (WN).

Neuregulin 1 type-I over-expression is associated with reduced NMDA receptor-mediated synaptic signaling in hippocampal interneurons expressing PV or CCK

Abbreviated Title: *NMDAR hypofunction in interneurons by NRG1 type-I*

Abstract

Hypofunction of *N*-methyl-D-aspartate receptors (NMDARs) in inhibitory GABAergic interneurons is implicated in the pathophysiology of schizophrenia (SZ), a heritable disorder with many susceptibility genes. However, it is still unclear how SZ risk genes interfere with NMDAR-mediated synaptic transmission in diverse inhibitory interneuron populations. One putative risk gene is neuregulin 1 (NRG1), which signals via the receptor tyrosine kinase ErbB4, itself a schizophrenia risk gene. The type-I isoform of *NRG1* shows increased expression in the brain of SZ patients, and ErbB4 is enriched in GABAergic interneurons expressing parvalbumin (PV+) or cholecystokinin (CCK+). Here, we investigated ErbB4 expression and synaptic transmission in interneuronal populations of the hippocampus of transgenic mice over-expressing NRG1 type-I ($NRG1^{tg\text{-}type\text{-}I}$ mice). Immunohistochemical analyses confirmed that ErbB4 was co-expressed with either PV or CCK in hippocampal interneurons, but we observed a reduced number of ErbB4-immunopositive interneurons in the $NRG1^{tg\text{-}type\text{-}I}$ mice. NMDAR-mediated currents in interneurons expressing PV (including PV+ basket cells) or CCK were reduced in $NRG1^{tg\text{-}type\text{-}I}$ mice compared to their littermate controls. We found no difference in AMPA receptor-mediated currents. Optogenetic activation (5 pulses at 20 Hz) of local glutamatergic fibers revealed a decreased NMDAR-mediated contribution to disynaptic GABAergic inhibition of pyramidal cells in the $NRG1^{tg\text{-}type\text{-}I}$ mice. GABAergic synaptic transmission from either PV+ or CCK+ interneurons, and glutamatergic transmission onto pyramidal cells, did not significantly differ between genotypes. The results indicate that synaptic NMDAR-mediated signaling in hippocampal interneurons is sensitive to chronically elevated NGR1 type-I

levels. This may contribute to the pathophysiological consequences of increased *NRG1* expression in SZ.

Significance statement

Hypofunction of NMDA receptors in inhibitory GABAergic interneurons is implicated in pathophysiology of schizophrenia (SZ), but it is largely unknown how SZ risk genes interfere with NMDAR-mediated signaling in specific interneurons. We investigated synaptic transmission in hippocampus of mice over-expressing the type-I isoform of the putative SZ risk gene, NRG1, and found markedly reduced NMDAR-mediated synaptic responses in GABAergic interneuron types labeled for PV or CCK which are known to express the NRG1 receptor ErbB4. The NMDAR hypofunction changed synaptic excitatory drive of interneurons during hippocampal network activity. The observed reductions of NMDAR-mediated transmission in these interneurons may contribute to the hippocampal dysfunction observed with increased NGR1 type-I expression, and may provide a link to the genetic predisposition to SZ.

Introduction

Many schizophrenia (SZ) susceptibility genes have been linked to *N*-methyl-D-aspartate receptor (NMDAR) signaling (Harrison and Weinberger, 2005; Hall et al., 2015) consistent with the hypothesis that NMDAR hypofunction contributes to the disease pathophysiology (Olney and Farber, 1995; Coyle, 2012; Gonzalez-Burgos and Lewis, 2012). It has been proposed that NMDAR function could particularly be impaired in hippocampal and neocortical GABAergic interneurons in the disorder compromising recurrent inhibition (Carlen et al., 2012; Curley and Lewis, 2012; Gilmour et al., 2012). Two prominent GABAergic inhibitory interneuron subpopulations, defined by mutually exclusive markers parvalbumin (PV) or cholecystokinin (CCK), are strongly involved through recurrent inhibition in rhythmic network activities in the neocortex and hippocampus (Cobb et al., 1995; Ellender and Paulsen, 2010; Manseau et al., 2010; Lasztoczi et al., 2011; Buzsaki and Wang, 2012; Fasano et al., 2017; Pelkey et al., 2017). Disrupted function of either of these interneuron populations in animal models results in alterations of co-ordinated neuronal network activities, particularly the synchronous gamma frequency (20-80 Hz) oscillations, and causes behavioral changes associated with the disorder (Belforte et al., 2010; Nakazawa et al., 2012; Brown et al., 2014; Schmidt et al., 2014; Cho et al., 2015; Gonzalez-Burgos et al., 2015; Schmidt and Mirnics, 2015; Huang et al., 2016; Del Pino et al., 2017; Medrihan et al., 2017; Vargish et al., 2017). However, whether and how specific SZ susceptibility genes interfere with NMDAR-mediated synaptic signaling in these interneurons is still not well known (Gonzalez-Burgos and Lewis, 2012; Vullhorst et al., 2015). In this respect the gene for neuregulin 1 (*NRG1*) is a relevant candidate to study because diverse evidence links it to NMDAR function and SZ pathogenesis (Stefansson et al., 2002; Corfas et al., 2004; Gu et al., 2005; Hahn et al., 2006; Law et al., 2006; Bjarnadottir et al., 2007; Chong et al., 2008; Pitcher et al., 2011; Weickert et al., 2013). Moreover, the main receptor for NRG1 signaling, ErbB4, itself a schizophrenia risk gene (Schizophrenia Working Group of the Psychiatric Genomics Consortium, 2014) is expressed in PV+ and in CCK+ GABAergic interneurons but not in glutamatergic

pyramidal cells (Vullhorst et al., 2009; Fazzari et al., 2010; Neddens et al., 2011; Del Pino et al., 2017).

NRG1 has several functionally distinct isoforms, of which type-I (among others) has been reported to be over-expressed in SZ (Hashimoto et al., 2004; Law et al., 2006). Over-expression of NRG1 type-I mRNA, or administration of the protein in early postnatal development, results in pathophysiological changes reminiscent of schizophrenia endophenotype in animal models: alterations in rhythmic gamma-frequency network oscillations (Deakin et al., 2012) and synaptic plasticity (Agarwal et al., 2014), and a behavioral phenotype including age-emergent impairment of hippocampal working memory (Chen et al., 2008; Deakin et al., 2009; Kato et al., 2011; Yin et al., 2013; Luo et al., 2014). These findings together suggest that NRG1-ErbB4 signaling may regulate glutamatergic NMDAR-mediated transmission in interneurons, and that alterations in this mechanism might contribute to the pathophysiology of SZ. To investigate this possibility, we have studied synaptic function in hippocampal interneurons expressing PV or CCK in mice over-expressing NRG1 type-1, using a combination of electrophysiological, optogenetic and immunohistochemical techniques.

Materials and methods

Ethics Statement: All animal procedures were performed in accordance with the British Home Office regulations and personal and project licenses held by the authors, following local ethical review at the University of Oxford (UK).

Experimental animals: Experiments were conducted on heterozygous (at least 1 month old) NRG1 type-I transgenic ($NRG1^{tg\text{-}type\text{-}I}$ +/-) mice of either sex, overexpressing NRG1 type-I (β1a-isoform) under a Thy-1.2 promoter (RRID:MGI:3530784) (Michailov et al., 2004). To specifically express fluorescent marker in PV interneurons, PV-Cre+/+ mice (The Jackson Laboratory, B6;129P2-Pvalbtm1[cre]Arbr/J) (RRID:IMSR_JAX:017320) were crossbred with Ai9+/+ mice (The Jackson Laboratory, B6.Cg-Gt[ROSA]26Sortm9[CAG-tdTomato]Hze/J) (RRID:IMSR_JAX:007909) to produce tdTomato expression in the PV+ cells (Figs. 1, 2 and 3). The female offspring were further crossed with the $NRG1^{tg\text{-}type\text{-}I}$ +/- males. For the experiments in Fig.4, Lhx6-eGFP+/- females expressing GFP in PV cells (The Jackson Laboratory, Tg[Lhx6-EGFP]BP221Gsat/M, RRID:MMRRC_000246-MU) were crossbred with male $NRG1^{tg\text{-}type\text{-}I}$+/- mice and anatomically identified basket cells in hippocampal slices (Nissen et al., 2010) were defined as PV+ basket cells (PVBCs) and confirmed immunonegative for axonal cannabinoid receptor type 1 (CB1R) (Armstrong and Soltesz, 2012). To express fluorescent marker in CCK neurons, heterozygous BAC-CCK-Cre tg mice (Geibel et al., 2014) (RRID:MGI:5575864) were crossed with the Ai9+/+ mice for tdTomato expression in the CCK+ cells. For the virus transduction studies, PV-Cre+/+ females (The Jackson Laboratory, B6;129P2-Pvalbtm1[cre]Arbr/J) (RRID:IMSR_JAX:017320), heterozygous BAC-CCK-Cre tg females (RRID:MGI:5575864) or CaMKII-Cre+/+ females (B6.Cg-Tg[Camk2a-cre]T29-1Stl/J) (RRID:IMSR_JAX:005359) were crossbred with male $NRG1^{tg\text{-}type\text{-}I}$+/- mice. The Cre-expressing $NRG1^{tg\text{-}type\text{-}I}$ and the control littermates were injected with adeno-associated virus construct encoding opsin.

Opsin construct transduction: Mice were anesthetized with 2-4 % isoflurane (CHEBI: 6015). AAV2-ChR2-eYFP (in some cases AAV5-ChR2-eYFP) was stereotactically injected via 33-gauge needle attached to a Microlitre Syringe (Hamilton) into mid-ventral CA3 or into dorsal CA1 hippocampus. The vector sequence was: pAAV-EF1a-sCreDIO hChR2(H134R)-EYFP-WPRE (Vector Core Services, Gene Therapy Centre Virus, University of North Carolina, USA). In each hemisphere, a craniotomy was performed using a micro torque, and a total volume of 800 nL of virus suspension (viral particle suspension titre 4 x 10^{12}/mL) was delivered at 80 nL / min by a Micro Syringe Pump Controller (World Precision Instruments). The scalp incision was sutured, and mice were allowed to recover for 10–21 days. Light exposure of brain tissue during preparation of slices was minimized to avoid photoactivation of ChR2. In experiments, ChR2 was activated by a fixed-spot laser (Laser nominal max power 100 mW; Rapp OptoElectronics) light (20 µm diameter to evoke IPSCs with minimal stimulation of GABAergic fibers, and 80 µm diameter in experiments stimulating glutamatergic fibers with 20 Hz train stimulation) via the microscope objective.

Identification of interneuron populations and pyramidal cells: CCK interneurons in Figure 1 were tagged by the fluorescent marker tdTomato using the crossed mouse line: BAC-CCK-Cre tg with Ai9 mice. In figure 2, CCK-expressing interneurons were identified with positive immunoreaction for somatic pro-CCK or by positive immunoreaction for axonal CB1R when the soma recovery was compromised. In figures 1, 2 and 3 the PV-expressing cells were identified by genetic fluorescence marker in PV-Cre mice crossed with Ai9 mice. Recorded cells were filled with neurobiotin (0.3 % w/v) and visualized, and some were anatomically identified as basket cells by their characteristic predominant axon distribution in *str. pyramidale* and the lack of axo-axonic cell axon terminal cartridges (Klausberger and Somogyi, 2008). In addition, the basket cells in figure 4 were confirmed immunonegative for axonal CB1R (Katona et al., 1999; Tsou et al., 1999; Bodor et al., 2005) (Armstrong and Soltesz, 2012). Pyramidal cells (PCs) were identified by their somatodendritic structure with mushroom spines along the dendrites.

176

177 *Electrophysiological recordings:* Mice were anesthetized with sodium-pentobarbitone and
178 decapitated. Following brain removal, horizontal (for mid-ventral hippocampus) or coronal (for
179 dorsal hippocampus) brain slices (250 µm) were cut using a vibrating microtome (Microm HM650V)
180 in oxygenated (95 % O_2/ 5 % CO_2) ice-cold (0 to 4 °C) cutting solution. The composition of the cutting
181 solution was (in mM): 75 sucrose, 87 NaCl, 2.5 KCl, 0.5 $CaCl_2$, 7 $MgCl_2$, 1.0 NaH_2PO_4, 25 $NaHCO_3$, 25
182 glucose, pH 7.4, bubbled with 95 % O_2/5 % CO_2. Slices were kept submerged at 32 °C in the sucrose
183 solution for 20–25 min before being transferred to an interface chamber in which they were
184 maintained in Earle's balanced salt solution (ThermoFisher Scientific, Cat# 14155063) with 3
185 mm Mg^{2+} and 1 mm Ca^{2+} at room temperature (20–24 °C) for at least 60 min before starting
186 experiments. In the experiments the slices were superfused with oxygenated recording solution at 5
187 mL / min in a submerged-type recording chamber at 30 °C (Luigs & Neumann) mounted on Olympus
188 BX51 microscope stage (20× objective, 2–4 zoom) with epifluorescence and filters (eGFP, eYFP,
189 tdTomato) and DIC-IR with a CCD camera (Till Photonics). The superfusion solution was (in mM): 119
190 NaCl, 2.5 KCl, 2.5 $CaCl_2$, 1.3 $MgSO_4$, 1.25 NaH_2PO_4, 25 $NaHCO_3$, and 11 glucose, final pH 7.4
191 (equilibrated with 95 % O_2/5 % CO_2).

192

193 Borosilicate-glass microelectrodes were pulled (P-97, Sutter Instrument) from GC150F-10 capillaries
194 (Harvard Apparatus). Pipettes (6-8 MΩ) were filled (Figs. 2, 3, 4) with (in mM): 145 Cs-
195 methanesulfonate, 20 HEPES, 10 CsOH, 8 NaCl, 0.2 CsOH-EGTA, 2 ATP-Mg, 0.3 GTP-Na, 5 QX-314,
196 and 0.2-0.5 % neurobiotin (295 mOsm, pH 7.2). In Figs. 5 and 6, 145 K-gluconate or K-
197 methanesulfonate (with 10 KOH, and 0.2 K-EGTA) were used instead. Recordings with >30 % change
198 in access resistance were excluded. Liquid-junction potential was not corrected. Data were recorded
199 with a Multiclamp 700B amplifier, low-pass filtered (cutoff frequency ≥2 kHz), digitized (≥10 kHz,
200 Digidata 1400), acquired by Clampex and analyzed by pClamp10.2 (Molecular Devices, SCR_011323).

201

Extracellular electrical stimuli were applied via a bipolar electrode (50-100 µs, 50-400 µA) in *stratum oriens* and current isolator (CBAPC75PL1, FHC) every 15 s. Synaptic currents were post-hoc low passed filtered at 1KHz. Pharmacologically isolated AMPA receptor (AMPAR)-mediated EPSC peak amplitude was recorded at -60 mV, and the NMDAR-mediated EPSC amplitude was measured in the presence of the AMPA/kainate receptor blocker NBQX at a membrane potential 40 mV positive to their measured reversal potential estimated by a linear fitting curve of the current- voltage relation for at least 20 evoked NMDAR EPSCs measured between -20 mV and +65 mV (Deleuze and Huguenard, 2016). In cells where no NMDAR EPSC was detected the current was defined as 0.

mEPSC recordings (2 min for AMPAR and 2 min for NMDAR mEPSCs) were acquired at 20 kHz and band-pass filtered off-line (cutoff frequencies 4 Hz–5 or 6 kHz at -65mV, 2-500 Hz at +40 mV) for analysis. Events were detected with an amplitude threshold-crossing algorithm in pClamp (Axon Instruments, SCR_011323). Criteria for threshold detection for NMDAR mEPSCs (at +40 mV) were: amplitude threshold 7 pA, duration 0.8-200 ms with noise rejection 0.8 ms. For the AMPAR mEPSCs (at -65 mV) the amplitude threshold was 5 pA, duration 0.5-100 ms with noise rejection 0.5 ms) evaluated after blockade of AMPARs with NBQX (25 µM). The same detection criteria were employed for all cells. Number of AMPAR mEPSCs investigated in the analyses were: In wild-type (WT) basket cells (median and quartile range) = 424 and 279-680 events (7 cells), in the $NRG1^{tg\text{-}type\text{-}I}$ mice basket cells = 394 and 301-470 events (6 cells), in the WT pyramidal cells = 134 and 128-205 events (7 cells), in the $NRG1^{tg\text{-}type\text{-}I}$ mice pyramidal cells = 95 and 64-150 events (10 cells). Number of NMDAR mEPSCs measured in similar time window were: In WT basket cells (median and quartile range) = 513 and 178-792 events (6 cells), in the $NRG1^{tg\text{-}type\text{-}I}$ mice basket cells = 348 and 280-520 events (6 cells). mEPSC frequency was calculated from the 2 min time window as the event occurrence in Hz. Average mEPSC amplitude was calculated in each cell from all events occurring in the 2 min time window.

In experiments using optogenetic stimulation of GABAergic fibers the monosynaptic IPSCs were measured at 0 to -10 mV. Optogenetic stimulation of the glutamatergic fibers (5 pulses at 20 Hz) was applied every 30 s while the disynaptic IPSCs were recorded (on average at +11 mV, see Results) in postsynaptic pyramidal cells. The optogenetically-evoked postsynaptic currents were low-pass filtered off-line at 1 kHz, and the evoked postsynaptic current charge was analyzed with pClamp10.2 (Molecular Devices, SCR_011323).

Drugs: Drugs were purchased as follows: 2,3-dioxo-6-nitro-1,2,3,4-tetrahydrobenzo[f]quinoxaline-7-sulfonamide disodium salt (NBQX) from Abcam ltd; DL-2-amino-5-phosphonopentanoic acid sodium salt (DL-AP5), picrotoxin (PiTX), CGP55845, 4-[(2*S*)-2-[(5-isoquinolinylsulfonyl)methylamino]-3-oxo-3-(4-phenyl-1-piperazinyl)propyl] phenyl isoquinolinesulfonic acid ester (KN-62) and (*RS*)-α-methyl-4-carboxyphenylglycine (MCPG) from Tocris Bioscience. Stocks were diluted (1:1000) in ddH_2O, DMSO or ethanol.

Statistics: A *t*-test was used for data that were normally distributed (Shapiro-Wilk test) and with $n \geq 10$ in tested groups. Otherwise, a Mann-Whitney U-test or Rank Sum test was used.

Anatomical and immunohistochemical processes: Following whole cell recordings, slices were fixed overnight at 4 °C in 4 % paraformaldehyde (NIFCHEM:birnlex 3072_2), 0.05 % glutaraldehyde (NIFINV:birnlex 3070_2) and 0.2 % picric acid in 0.1 M sodium phosphate buffer (PB), then washed in 0.1 M PB. Slices were embedded in 20 % gelatine and sectioned (40–60 µm) with a microtome (Leica VT1000) in 0.1 M PB, then washed in 50 mM Tris-buffered saline (TBS, pH 7.4) with 0.3 % Triton X-100 (TBS-Tx) and incubated with streptavidin-Alexa Fluor488 (1:2000, Invitrogen, Cat# S-32354) or -Cy3 (1:2000, Thermofisher, Cat# S-A1010), and finally washed in 50 mM TBS-Tx. Sections mounted in Vectashield (Vector Laboratories) were examined with an epifluorescence microscope (DM5000-B, Leica Microsystems) using appropriate filter sets and a CCD camera (ORCA-ER, Hamamatsu).

Sections for immunoreactions were washed in 50 mM TBS-Tx, blocked in 20 % normal horse serum (NHS, Vector Laboratories) in TBS-Tx for at least 1 hour at room temperature (20-24 °C), and incubated in primary antibodies for 48 hours at 4 °C in TBS-Tx with 1% NHS. Fluorochrome-conjugated secondary antibodies were applied overnight at 4 °C in TBS-Tx with 1% NHS. Mounted sections in Vectashield were evaluated at ≥40× magnification using confocal laser-scanning microscopy (LSM710, Carl Zeiss) with Zen2008 software. Digital micrographs were constructed from z-stacks with Image-J software (SCR:003070). Micrographs were only adjusted for brightness and contrast. The primary antibodies used were: rabbit anti-ErbB4 (Polyclonal anti-antiserum 5941, 1:500) (Vullhorst et al., 2009), guinea pig anti-PV (Synaptic Systems, Cat# 195004, RRID:AB_2156476, 1: 2000), rabbit anti-proCCK (RRID:AB_2571674, 1:500) (Morino et al., 1994), guinea pig anti-CB1R (Frontier Science ltd. Cat# CB1-GP-af530-1, RRID:AB_2571593, 1:1000). The secondary antibodies were: CY5 donkey anti-guinea pig (1:250, Jackson immunoResearch, Cat# 706-175-148), CY3 donkey anti-guinea pig (1:400, Jackson immunoResearch, Cat# 706-165-148), Alexa 647 donkey anti-guinea pig (1:250, Invitrogen, Cat# 706-605-148), Alexa 488 donkey anti-rabbit (1:500, Invitrogen, Cat# A21206), Dylight 649 donkey anti-rabbit (1:250, Jackson immunoResearch, Cat# 711-495-152).

Cell density analyses: Mice were anesthetized with 2-4 % isoflurane (CHEBI:6015) at a rate of 1.0-1.5 ml/min and then further anesthetized with intraperitoneal injection of pentobarbitone sodium (20 % w/v, dosage 0.2 mg/g; Pharmasol, Andover, UK). Animals were perfused with 0.1 M phosphate buffered saline solution (PBS, pH 7.4, at 22-24°C) followed by ice-cold fixative solution; 4 % w/v paraformaldehyde (PFA, NIFCHEM:birnlex 3072_2) with 15 % v/v saturated picric acid solution in 0.1 M PB. Vibratome (VT1000S Leica Microsystems, UK) was used for cutting coronal brain sections (60 µm thickness). Sections containing the hippocampal formation were washed (3-5 times, 10 min) with TBS-Tx and blocked with 20 % normal horse serum (NHS) in TBS-Tx for 1 hour at room temperature (20-24 °C). This was followed by a two night incubation with the primary antibodies: rabbit anti-ErbB4 (Polyclonal anti-antiserum 5941, 1:500) and guinea pig anti-PV (synaptic systems Cat# 195004,

RRID:AB2156476, 1: 2000) in TBS-Tx with 1 % NHS at 4 °C. After washes (3-5 times, 10 min each) with TBS-Tx, sections were incubated overnight with Alexa 488-conjugated and Alexa 647-conjugated secondary antibodies both raised in donkey, respectively in TBS-Tx with 1 % NHS. Sections containing mid-ventral hippocampus from both hemispheres were scanned using an epifluorescence microscope (AxioImager M2; Zeiss) equipped with Stereoinvestigator software (MBF Bioscience). Optical sections of 1 µm were acquired using a 20× objective at a final depth of 20 µm from the section surface, whilst the first 1 µm from the section surface was defined as a guard zone and not scanned (Bocchio et al., 2015). Brightness and contrast acquiring settings were adjusted for each section, in order to achieve good visualization of all positive cells for a specific neuromarker across all sections areas. Cell counting was performed off-line. Distinct hippocampal regions were visually delineated and analyzed as individual anatomically defined subregions as follows: CA1-2 alveus (alv)/stratum oriens (s.o)/stratum pyramidale (s.p), CA1-2 stratum radiatum (s.r)/stratum lacunosum-moleculare (s.l-m), CA3 alv/s.o/s.p and CA3 stratum lucidum (s.l)/s.r/s.l-m. Cells were counted when the cell somata or nuclei came into focus with the optical dissector.

Immunoblotting: Tissue sample homogenates were prepared from mouse hippocampus in ice cold lysis buffer containing 20 mM Tris (PH= 7.5), 50mM NaCl, 1 mM EDTA, 0.1 % SDS, 1 % Triton X-100, 2 % protease inhibitors (Roche), 1 % phosphatase inhibitors Cocktail 2 and 3 (Sigma), using a plastic homogenizer, repeated passages through a syringe, followed by 5 minute sonication and a 75 minutes rotation at 4 °C. Next, the homogenates were centrifuged at 4000G and the supernatant was collected. Lysates were quantified for their total protein content with standard Bradford assay (Bio-Rad ltd.) and diluted to sample buffer containing 100 mM (or 2× increased) DTT, 10 % glycerol, 2 % SDS, 2 mM Tris HCl and 0.1 % (w/v) bromophenol blue crystals and incubated at 95 °C for 5 min to denature proteins. Protein lysates were size separated by SDS-PAGE, using a 6 % or 10 % acrylamide gels and electrophoretically transferred onto nitrocellulose membranes. After blocking in the Odyssey proprietary blocking buffer (LI-COR Biosciences) for 1 h at room temperature (20-24 °C),

306 membranes were incubated with the primary antibodies overnight at 4 °C (rabbit anti-ErbB4,
307 polyclonal anti-antiserum 5941, 1:900). Rabbit anti-glyceraldehyde 3-phosphate dehydrogenase
308 (GADPH), 1:10000) in Odyssey blocking buffer was supplemented with 0.01 % tween 20. Following
309 washes with PBS x Tx (5 times, 5 min), membranes were incubated with the appropriate fluorescent
310 secondary antibody (goat anti-rabbit IRDYe 800CW, LI-COR Biosciences ltd.) for 1 hour at 20-24 °C.
311 Finally, after (5 times, 5 min) washes with PBS x Tx, the membranes were scanned with an infrared
312 scanner (Odyssey Clx scanner, LI-COR Biosciences, SCR:014579) and the digital scans were analyzed
313 with the Image Studio Lite software (LiCor ltd, SCR:014211).
314
315 **Results**
316
317 **Expression of ErbB4 in the hippocampus of wild-type and NRG1 type-I over-expressing mice**
318
319 Given the well-established role of ErbB4 as the major receptor to elicit NRG1 signaling cascades in
320 the brain (Flames et al., 2004; Lopez-Bendito et al., 2006; Krivosheya et al., 2008; Fazzari et al., 2010;
321 Li et al., 2012b), we visualised the ErbB4 receptor in hippocampal interneurons using rabbit anti-
322 ErbB4 (polyclonal anti-antiserum 5941) immunostaining, which shows high epitope specificity
323 (Vullhorst et al., 2009). We found that ErbB4 co-expressed with PV and CCK, the mutually exclusive
324 neuronal markers (Fig. 1A1-2) which label perisoma (and also some dendrite) -targeting hippocampal
325 interneuron types. Given that NRG1-ErbB4 signaling is known to regulate interneuron migration,
326 survival and proliferation during neurodevelopment (Flames et al., 2004; Li et al., 2012b), we first
327 investigated whether the NRG1 type-I over-expressing mice showed an altered distribution of
328 ErbB4+ interneurons in the hippocampus. Fluorescence imaging-based ErbB4+ cell soma counting
329 showed a reduced density in the $NRG1^{tg\text{-}type\text{-}I}$ mice compared to the WT mice in all subfields (Fig.1B1,
330 Fig.1B2). In the whole hippocampus (including the CA1-CA3 areas) of the WT mice, the ErbB4+ soma
331 density was 4.98×10^3 cells/mm^3 (median, interquartile range 4.65 to 5.66 x 10^3 cells/mm^3) and in

the NRG1$^{tg\text{-}type\text{-}I}$ mice 2.82 × 10^3 cells/mm^3 (median, interquartile range 2.37 to 3.48 x 10^3 cells/mm^3) (p = 0.002, Mann Whitney U-test) (Fig.1B2). Hippocampal sub-regions, compared separately, were defined as follows: 1) *stratum pyramidale* with infrapyramidal laminae in the CA1-2 area, 2) suprapyramidal layers in the CA1-2 area, 3) *stratum pyramidale* with infrapyramidal laminae in the CA3 area, 4) suprapyramidal layers in the CA3 area. The sub-region specific soma counting results are illustrated in Fig. 1B2. The cell counts in the CA1 and CA2 areas were pooled together because of small size of the CA2, and the result mainly represents the CA1 area.

In contrast, analysis of PV-immunopositive cell somata showed no difference between the two genotypes, in line with a previous study using the same NRG1$^{tg\text{-}type\text{-}I}$ mouse line (Deakin et al., 2012). Fluorescence imaging-based PV+ cell soma counting (Fig. 1C1) in the WT mice revealed 2.44 × 10^3 cells/mm^3 (median, interquartile range 2.03 to 2.74 × 10^3 cells/mm^3, n = 9 sections in 3 mice) (Fig.1C2). Correspondingly, the PV+ cell soma density analysis in the NRG1$^{tg\text{-}type\text{-}I}$ mice showed 2.28 × 10^3 cells/mm^3 (median, interquartile range 2.03 to 2.63 × 10^3 cells/mm^3, n = 12 sections in 3 mice) (p = 0.696, Mann Whitney U-test) (Fig.1C1-2). The detected PV+ cell densities were also unaltered in the analyzed hippocampal sub-regions (Fig.1C2). When we quantified percentages of the ErbB4 and PV co-expressing neurons in the two genotypes, we found that in both genotypes most hippocampal PV+ cells co-expressed the ErbB4 receptor (Fig.1D1). Comparing the co-expression results in the entire hippocampus did not show difference between the genotypes (Fig.1D2). In WT mice the co-expression covered 77.66 % (median, interquartile range 75.85 - 86.85 %, n = 9 slices from 3 mice) of the PV+ neurons; in the NRG1$^{tg\text{-}type\text{-}I}$ mice it comprised 75.64 % (median, interquartile range 72.41-80.01 %, n = 12 slices from 3 mice) of the PV+ cells (p = 0.166, Mann-Whitney U-test) in agreement with previous studies (Yau et al., 2003; Fazzari et al., 2010; Bean et al., 2014 see also Neddens and Buonanno, 2010). However, when comparing the expression in the hippocampal subareas (Fig. 1D2), a significant but small decrease was observed in the co-expression level specifically in the CA1-2 area

(including *alveus*, *stratum oriens* and *stratum pyramidale*) in the NRG1$^{tg\text{-}type\text{-}I}$ mice (p = 0.043, Mann Whitney U-test) (Fig.1D2).

These results show that the NRG1 type-I over-expression does not produce significant changes in the co-expression of ErbB4 and PV in most hippocampal areas nor in the spatial distribution of PV+ neurons in the hippocampus. Yet, these data suggest that the NRG1 over-expression leads to altered ErbB4+ cell soma count of interneurons other than those expressing PV. This could emerge either from changes in the migration, survival and proliferation of these cells during neurodevelopment (Flames et al., 2004; Li et al., 2012a) or be caused by alterations in the expression and trafficking of the receptor (Longart et al., 2007) (see Discussion).

We found no significant difference in ErbB4 protein levels between the two genotypes using western blot analysis of whole hippocampus extracts (n = 6 including 3 males and 3 females in both genotypes, p = 0.310, Mann-Whitney U-test) (Fig.1E1-3). This discrepancy may partly be attributed to the fact that the cell density analysis focused on cells in specific hippocampal subregions, whereas the lysates in the immunoblots comprised the entire hippocampus, possibly masking subregion specific differences (see Discussion).

In conclusion the above results suggest that expression level or pattern of the ErbB4 in some hippocampal CA1 and CA3 cells is altered in response to the NRG1 type-I genomic over-expression (see Discussion). In addition, the analyses confirm earlier findings that ErbB4 is present in the hippocampal interneurons expressing PV or CCK (Vullhorst et al., 2009), and that both, PV+ and the PV- interneuron sub-populations expressing the receptor ErbB4 are present in the NRG1$^{tg\text{-}type\text{-}I}$ mouse hippocampus (see Fig. 1B2).

Hippocampal interneurons expressing parvalbumin or cholecystokinin have reduced synaptic NMDAR-mediated currents in the mice over-expressing NRG1 type-I

Next, we studied synaptic AMPAR- and NMDAR-mediated glutamatergic EPSCs in three neuron subpopulations in the CA3 area of acute hippocampal slices; PV+ interneurons (Fig. 2A1), CCK+ interneurons (Fig. 2A2), which both commonly express the ErbB4 (see Fig. 1), and pyramidal cells in which the receptor is absent (Vullhorst et al., 2009). All cells were studied in the whole-cell voltage clamp mode in hippocampal slices from mice expressing fluorescent marker (tdTomato) in PV-interneurons (see Materials and methods). The CCK+ GABAergic interneurons were identified *post hoc* by positive immunoreaction for cytoplasmic pro-CCK (tested when cell soma was recovered, n = 3 in WT control and n = 4 in the $NRG1^{tg\text{-}type\text{-}I}$ mice) or axonal CB1R (tested when only interneuron axon was recovered, n = 7 and n = 7 respectively) (Fig.2A2) (Katona et al., 1999). We applied electrical microelectrode stimulation in the CA3 *stratum oriens* aiming to activate predominantly associative-commissural fibers. Blockers for $GABA_A$ and $GABA_B$ receptors (picrotoxin, 100 µM and CGP55845, 1 µM) were present in all experiments. We found that the NMDAR-mediated EPSCs in PV+ interneurons of the $NRG1^{tg\text{-}type\text{-}I}$ mice were smaller, in comparison to the AMPAR EPSCs, than in their WT littermate controls (measuring a ratio of the NMDAR-EPSC and the AMPAR-EPSC amplitude, N/A ratio) (Fig. 2B1). The evoked average glutamatergic EPSCs in the $NRG1^{tg\text{-}type\text{-}I}$ mice were (median, interquartile range): NMDA EPSC = 19.8 pA, 10.4 - 45.5 pA, and AMPAR EPSC = 110.7 pA, 79.1 - 136.0 pA. Correspondingly, the N/A ratio in the $NRG1^{tg\text{-}type\text{-}I}$ mice was 0.18, 0.08 - 0.29 (n = 29). In the WT control mice the NMDA EPSC amplitude was 47.6 pA (median, interquartile range 29.1 - 60.8 pA), and the AMPAR EPSC amplitude 127.8 pA, 79.6 - 214.7 pA. Hence the N/A ratio in WT was 0.28, 0.19 - 0.42 (n = 38). The N/A ratios in PV+ cells of the two genotypes were different (p = 0.010, Mann-Whitney U-test). Fig.2B2 shows cumulative histograms of the N/A ratios measured in the PV+ interneurons of the two genotypes.

Likewise, we found that the CCK+ CA3 area interneurons in the NRG1$^{tg\text{-}type\text{-}I}$ mice showed smaller N/A amplitude ratio (median 0.57, interquartile range 0.46 - 0.98, n = 12) than their littermate controls (median 1.12, interquartile range 0.82 - 1.25, n = 10) (p = 0.019, Mann-Whitney U-test) (Fig.2C1). The EPSC amplitudes in the CCK+ interneurons in the NRG1$^{tg\text{-}type\text{-}I}$ mice were (median, interquartile range): NMDAR EPSC = 31.8 pA, 26.4 - 43.8 pA, and AMPAR EPSC = 54.9 pA, 30.8 - 65.9 pA (n = 12). In the WT mouse CCK+ cells the NMDAR EPSC was 52.6 pA (median, interquartile range 37.1 - 73.6 pA) and the AMPAR EPSC was 42.5 pA (median, interquartile range 33.2 - 58.4 pA) (n = 10). Sample EPSCs in the CCK+ interneurons are illustrated in Fig. 2C1, and the cumulative histograms of the N/A ratios are shown in Fig.2C2. In line with previous observations, CCK+ interneurons had larger NMDAR-mediated synaptic currents (compared as the N/A ratio in the WT mice) than PV+ cells (p = 0.001, Mann-Whitney U-test) (Maccaferri and Dingledine, 2002; Matta et al., 2013).

In contrast to the interneurons, there was no difference in the N/A ratio across pyramidal cells (PCs) between genotypes (Fig.2D1-2 p = 0.761, Mann-Whitney U-test). EPSCs in the NRG1$^{tg\text{-}type\text{-}I}$ mice PCs were (median, interquartile range): NMDAR EPSC = 47.5 pA, 34.0 - 76.2 pA, and AMPAR EPSC = 63.8 pA, 41.9 -105.1 pA. Consequently, the N/A ratio in the NRG1$^{tg\text{-}type\text{-}I}$ mice was 0.80, 0.49 - 1.11 (n = 21). Correspondingly, in the WT mice the NMDA EPSC amplitude was 73.3 pA (median, interquartile range 45.0 - 96.5 pA), and AMPAR EPSC amplitude 100.1 pA (median, interquartile range 49.1 - 120.2 pA). The N/A ratio in the WT PCs was 0.79, 0.63 - 0.98 (n = 22).

Because both interneuron populations comprise various specialized cell types (Klausberger and Somogyi, 2008; Pelkey et al., 2017), and glutamatergic synapse features may vary between individual interneuron types (Papp et al., 2013) we visualized and anatomically examined the recorded interneurons (filled with neurobiotin) to identify basket cells (PVBCs) (Fig.3A) in the PV+ subpopulation (see Fig.2B). We confirmed 22 PVBCs (12 in the WT mice and 10 in the NRG1$^{tg\text{-}type\text{-}I}$ mice). Interestingly, the PVBC group in both genotypes showed parametric distribution of the N/A

values (in the NRG1$^{tg\text{-}type\text{-}I}$ mice W = 0.91, p = 0.270, and in the WT mice W = 0.96, p = 0.780) (Shapiro-Wilk test) showing that the N/A values have less variation in an identified PV+ cell type subpopulation than in the entire PV+ cell population in general. The PVBC data showed smaller N/A EPSC ratio in the NRG1$^{tg\text{-}type\text{-}I}$ mice (0.14 ± 0.04, n = 10) than in the WT control mice (0.31 ± 0.04, n = 12) (p = 0.006, mean ± s.e.m, t-test) (Fig.3B1-2). In addition to the basket cells, we identified two axo-axonic cells (Nissen et al., 2010) in the NRG1$^{tg\text{-}type\text{-}I}$ mice (their average N/A ratios 0.09 and 0.21) and one in the WT control littermates (N/A ratio = 0.18). Because of their low number, these cells were not separately compared between the genotypes (but the cells were included in the PV+ cell pool in Figure 2).

Quantal current analysis in parvalbumin basket cells shows unaltered AMPAR-mediated transmission in NRG1$^{tg\text{-}type\text{-}I}$ mice

Because the decreased N/A ratio alone is unable to distinguish between suppressed NMDAR currents and increased AMPAR EPSCs, and because altered NRG1 levels can affect AMPAR-mediated transmission (Abe et al., 2011), we next studied glutamatergic miniature currents (mEPSCs) in a new set of identified PVBCs recorded in the CA3 area (Fig.4A1). The cells were voltage clamped at -65 mV for the AMPAR EPSCs and at +40 mV for the NMDAR EPSCs in presence of tetrodotoxin (TTX, 1 µM) and the GABA receptor blockers (picrotoxin, 100 µM and CGP55845, 1 µM). In WT mice PVBCs, the AMPAR-mediated mEPSCs (Fig.4A2) occurred at 3.53 Hz (median, interquartile range 2.32 - 5.67 Hz, n = 7) and had amplitude of 28.9 pA (median, interquartile range 25.3 - 32.6 pA, n = 7). Correspondingly, in the NRG1$^{tg\text{-}type\text{-}I}$ mice the AMPAR mEPSCs (Fig.4A3) frequency was 3.28 Hz (median, interquartile range 2.51 - 3.92 Hz, n = 6) and the amplitude 28.3 pA (median, interquartile range 24.8 - 34.7 pA, n = 6). Neither the AMPAR mEPSC frequency (p = 0.954) nor the amplitude (p = 1.00) differed between the genotypes in the PVBCs (Mann-Whitney U-test).

460 In addition, we measured the NMDAR-mediated mEPSCs in the same identified PVBCs following
461 wash-in of NBQX (25 μM). One recording was lost before the NBQX application and therefore the n
462 number is smaller than above. We found that the frequency of detected NMDAR mEPSCs was not
463 different between WT PVBCs (Fig.4A4) (4.27 Hz, 1.48 - 6.60 Hz, n = 6) and the NRG1$^{tg\text{-}type\text{-}I}$ PVBCs
464 (Fig.4A5) (2.90 Hz, 2.34 - 4.33 Hz, n = 6) (median and interquartile range, p = 0.589, Mann-Whitney
465 U-test) (Fig.4A6). Yet, the amplitude of the NMDAR mEPSCs in NRG1$^{tg\text{-}type\text{-}I}$ mice (19.0 pA, 17.6 - 20.1
466 pA) (median, interquartile range) was moderately but significantly lower than in WT littermates
467 (21.8 pA, 20.8 - 30.0 pA) (p = 0.026, Mann-Whitney U-test). These results are summarized in Fig.4A6-
468 7.
469
470 We also recorded mEPSCs in the CA3 area PCs and found that neither AMPAR- nor NMDAR-
471 mediated mEPSCs differed between the genotypes. In the WT PCs, the AMPAR mEPSC (Fig.4B1)
472 values were 1.15 Hz (median, interquartile range 1.10 - 1.70 Hz, n = 7) and 20.8 pA (median,
473 interquartile range 18.8 - 21.9 pA, n = 7). Correspondingly, in the NRG1$^{tg\text{-}type\text{-}I}$ mice (Fig.4B2), the
474 values were 0.79 Hz (median, interquartile range 0.54 - 1.25 Hz, n = 10, p = 0.223 vs. the WT PCs) and
475 21.6 pA (median, interquartile range 19.0 - 25.0 pA, n = 10, p = 0.354 vs. the WT PCs) (Mann-Whitney
476 U-test). Respectively, the NMDAR mEPSCs in the WT PCs (Fig.4B3) occurred at 2.54 Hz (median,
477 interquartile range 1.60 - 3.71 Hz, n = 5) with amplitude of 18.5 pA (median, interquartile range 17.8
478 - 24.1 pA, n = 5). The NMDAR mEPSCs in the NRG1$^{tg\text{-}type\text{-}I}$ PCs (Fig.4B4) occurred at 1.94 Hz (median,
479 interquartile range 1.71 - 2.87 Hz, n = 9, p = 0.689 vs. the WT PCs) showing an amplitude of 19.3 pA
480 (median, interquartile range 18.5 - 20.6 pA, n = 9, p = 0.790 vs. the WT PCs). The results are
481 summarized in Fig.4B5-6.
482
483 The findings of unchanged AMPAR mEPSCs in the PVBCs and the PCs (and the moderate reduction of
484 the NMDAR mEPSC amplitude specifically in the PVBCs in the NRG1$^{tg\text{-}type\text{-}I}$ mice) indicate that the

485 altered N/A ratio observed (Fig.3) was caused by reduced postsynaptic NMDAR currents in the
486 NRG1$^{tg\text{-}type\text{-}I}$ mice PVBCs.
487
488 **GABAergic inhibitory currents from parvalbumin- or cholecystokinin-expressing CA3 interneurons**
489 **are not altered in NRG1$^{tg\text{-}type\text{-}I}$ mice**
490
491 Given that alterations in NRG1 levels can acutely change inhibitory synapses and modify them long-
492 term (Okada and Corfas, 2004; Woo et al., 2007; Chen et al., 2010; Yin et al., 2013; Agarwal et al.,
493 2014), we studied whether GABAergic synaptic output from interneurons expressing either PV or
494 CCK is also altered in the NRG1$^{tg\text{-}type\text{-}I}$ mice. To selectively stimulate axons from these interneurons,
495 we prepared slices from NRG1$^{tg\text{-}type\text{-}I}$ and WT mice expressing Cre-protein either in PV+ cells or CCK+
496 interneurons and transduced with a Cre-dependent adeno-associated virus (AAV)-channelrhodopsin-
497 2 (ChR2)-eYFP construct (see Materials and methods). Expression of the construct in the two types
498 of GABAergic fibers is illustrated in Fig.5A1-2. GABAergic IPSCs were elicited in the CA3 area
499 pyramidal cells stimulating the interneuron axons locally with brief laser light pulses (3 ms, 473 nm)
500 focused in *stratum pyramidale*. Stimulation intensity was set to use minimal laser power required for
501 stable IPSCs (Fig. 5B). In all experiments the postsynaptic pyramidal cells (voltage clamped at 0 to
502 +10 mV) were recorded in the presence of glutamate receptor blockers NBQX (25 µM) and DL-AP5
503 (100 µM). The optically evoked IPSCs were blocked with picrotoxin (100 µM) in all experiments
504 tested (n = 8 of 8 in IPSCs from PV+ fibers, and = 3 of 3 from CCK+ fibers).
505
506 We found that the IPSCs did not differ significantly between the genotypes for either PV+ or CCK+
507 GABAergic synapses (Mann-Whitney U-test). For PV+ fibers, the evoked IPSC amplitudes (Fig.5C1)
508 were 43.6 pA, 34.3 - 82.0 pA (median, interquartile range; n = 18 cells) in WT mice, and 44.8 pA, 36.2
509 - 82.7 pA in NRG1$^{tg\text{-}type\text{-}I}$ mice (n = 16 cell, p = 0.74 vs. the WT) (Fig.5C2). The IPSC rise time (from 20 %
510 to 80 % of the peak) values in the WT were 0.88 ms, 0.76 - 1.20 ms (n = 18 cells), and in the NRG1$^{tg\text{-}}$

$^{type-I}$ mice 0.97 ms, 0.87 - 1.49 ms (n = 16, p = 0.208 vs. the WT) (Fig.5C3). The IPSCs from the WT mice PV+ fibers showed a decay half-time of 9.4 ms, 8.6 - 12.4 ms (n = 18), and the decay half times in the NRG1$^{tg\text{-}type\text{-}I}$ PV+ cells were 10.1 ms, 9.0 - 12.8 ms (n = 16, p = 0.32 vs. the WT) (Fig.5C4). The paired-pulse ratio (PPR, 50 ms interval, 2nd IPSC/1st IPSC amplitude) in the WT mice was 0.69, 0.60 - 0.79 (n = 18), and in the NRG1$^{tg\text{-}type\text{-}I}$ 0.58, 0.80 - 0.76 (n = 16, p = 0.173 vs. the WT) (Fig. 5C5).

The IPSC amplitudes evoked from the CCK+ fibers (Fig.5D1) were 38.0 pA, 23.9 - 45.4 pA in WT mice (n = 5), and 23.4 pA, 18.0 - 44.7 pA in NRG1$^{tg\text{-}type\text{-}I}$ mice (n = 6, p = 0.662 vs. the WT) (Fig.5D2). The IPSC rise time (from 20 % to 80 % of the peak) in the WT mice was 2.40 ms, 1.40 - 3.60 ms (n = 5 cells), and 3.30 ms, 1.29 - 4.30 ms in the NRG1$^{tg\text{-}type\text{-}I}$ mice (n = 5, p = 0.94 vs. the WT) (Fig.5D3). The decay half time in the WT was 7.7 ms, 6.3 - 12.2 ms (n = 5), and in the NRG1$^{tg\text{-}type\text{-}I}$ mice it was 7.4 ms, 3.4 - 12.3 ms (n = 6, p = 0.79 vs. the WT) (Fig.5D4). The IPSCs evoked from the CCK+ fibers showed PPR of 0.61, 0.32 - 0.66 in WT (n = 5), and 0.75, 0.54 - 1.22 in the NRG1$^{tg\text{-}type\text{-}I}$ mice (n = 6, p = 0.33 vs. WT) (Fig.5D5).

Reduced NMDAR-driven recurrent inhibition in the hippocampus in NRG1$^{tg\text{-}type\text{-}I}$ mice

Finally, we investigated whether the reduced synaptic NMDAR-mediated transmission in these two common recurrent inhibition interneuron subpopulations had consequences for the GABAergic inhibition evoked by repetitive firing of the hippocampal glutamatergic neurons. To study this we optogenetically stimulated glutamatergic fibers focusing the laser light pulses in *stratum pyramidale* and *stratum oriens* aiming to activate the recurrent disynaptic GABAergic pathway. We did the experiments in the CA1 area to avoid polysynaptic glutamatergic discharge generated in the CA3 recurrent glutamatergic circuits (Maccaferri and McBain, 1995). We used hippocampal slices of the NRG1$^{tg\text{-}type\text{-}I}$+/-mice and their littermate WT controls both crossed with CaMKII-Cre+/- and transduced with the AAV-ChR2-eYFP construct in the hippocampus (Fig.6A). We made a translaminar

surgical cut in the slices from *alveus* to *stratum lacunosum-moleculare* in the CA1-CA2 area border to exclude the CA3 area recurrent excitatory loop and polysynaptic discharges (Maccaferri and McBain, 1995).

We applied bursts of five pulses of stimuli at 20 Hz every 60 seconds to generate disynaptic IPSCs in the CA1 area pyramidal cells. The IPSCs were recorded at a reversal potential of the EPSCs (+11.1 ± 0.7 mV, mean ± s.e.m.) elicited in the same cells (n = 13 comprising 7 cells in the NRG1$^{tg\text{-}type\text{-}I}$ mice and 6 cells in the WT controls) (Fig.6B1-2). Long-term plasticity blockers KN-62 (3 µM) and MCPG (200 µM) were present in all experiments for long-term stability of the disynaptic IPSCs (Perez et al., 2001; Kullmann and Lamsa, 2011; Campanac et al., 2013). Following stable baseline (at least 5 minutes), NMDAR blocker DL-AP5 (100 µM) was washed in (Fig. 6C1-2). This suppressed the evoked recurrent GABAergic IPSC in the WT mice to 0.66 of baseline (charge median, interquartile range 0.61 - 0.71, p = 0.031 vs. baseline, n = 6 cells), and in the NRG1$^{tg\text{-}type\text{-}I}$ mice to 0.74 (charge median, interquartile range 0.66 - 0.83, p = 0.026 vs. baseline, n = 7 cells) compared to the baseline (Mann Whitney Rank Sum -test). The IPSC charge was compared in each experiment between the last 3 min in baseline, and in an equal time window in the presence of DL-AP5 (at 5-8 min after DL-AP5 application). The suppression of the disynaptic IPSCs by the NMDAR blocker was larger in the WT than in the NRG1 mice (p = 0.014, Mann-Whitney U-test). The IPSCs were fully blocked at the end by NBQX (25 µM) in all experiments tested to verify their disynaptic origin (n = 4 in the WT controls, and n = 4 in the NRG1$^{tg\text{-}type\text{-}I}$ mice).

The results, summarized in Fig. 6D, indicate smaller NMDAR-mediated excitatory drive of hippocampal GABAergic interneurons in the NRG1$^{tg\text{-}type\text{-}I}$ mice compared to their WT littermates.

Discussion

563 Our results show that transgenic over-expression of NRG1 type-I, an isoform of NRG1 which has
564 elevated levels in some patients with SZ (Hashimoto et al., 2004; Law et al., 2006; Chong et al.,
565 2008; Weickert et al., 2012) (see also Boer et al., 2009; Parlapani et al., 2010; Hahn, 2011), is
566 associated with a hypofunction of NMDAR-mediated synaptic signaling in two major GABAergic
567 interneuron populations in mouse hippocampus.
568
569 The reduced ratio of NMDAR- to AMPAR-mediated synaptic currents was observed in the
570 hippocampal GABAergic interneuron populations expressing either PV or CCK, but not in PCs. This
571 finding on cell type-specificity is in line with the cortical ErbB4 expression pattern: various studies
572 have demonstrated that ErbB4 expression is predominant in GABAergic interneurons whereas it is
573 absent in PCs (Vullhorst et al., 2009; Fazzari et al., 2010; Neddens and Buonanno, 2010; Abe et al.,
574 2011; Pitcher et al., 2011; Del Pino et al., 2017). As illustrated in figure 1, we confirmed here the
575 ErbB4 expression in both PV+ and CCK+ interneurons, as has been previously reported (Vullhorst et
576 al., 2009). It should be noted that because of contrast adjustment, the figure 1A2 shows low CCK-Cre
577 -dependent fluorophore intensity in the CA3 pyramidal cells compared to interneurons although CCK
578 is expressed in both cell populations (Burgunder and Young, 1990; Geibel et al., 2014; Rombo et al.
579 2015).
580
581 ErbB4+ interneurons expressing either PV or CCK were found in the $NRG1^{tg\text{-}type\text{-}I}$ mice, but the cell
582 soma counting analysis indicated that the density of ErbB4+ neurons *not* co-expressing PV is reduced
583 in the hippocampus of NRG1 type-I over-expressing mice. This suggests that in some interneurons
584 either the ErbB4 receptor abundance has changed, or that detectable ErbB4 immunoreactivity has
585 decreased (e.g. due to an altered subcellular localization, or a change in epitope accessibility).
586 Surprisingly, western blot did not detect the reduction of ErbB4 expression although the detectable
587 ErbB4+ neuron soma number was reduced. We offer two possible explanations to this. The counting
588 of immunohistochemically-revealed ErbB4+ cell somata is a non-quantitative method (giving cells

589 clearly ErbB4+ or cells not confirmed positive). If the antibody-labeled fluorescence signal in the
590 soma is low, it becomes increasingly challenging to confirm it as immunopositive compared to
591 background. This could happen in the NRG1 type-I over-expressing mice without a significant change
592 in total hippocampal ErbB4 protein level, if subcellular location of the ErbB4 changed (decreased in
593 soma) or the ErbB4 protein is internalized in some interneurons (Liu et al. 2007, Longart et al. 2007)
594 making its detection by the antibody less evident. The discrepancy may also be attributed to the fact
595 that the cell density analysis focused on cells in specific hippocampal subregions, whereas the
596 lysates in the immunoblots comprised the entire hippocampus, possibly masking subregion-specific
597 differences.
598
599 We found that synaptic NMDAR currents were reduced in interneurons expressing PV or CCK, but
600 not in pyramidal cells in the $NRG1^{tg\text{-}type\text{-}I}$ mice. Furthermore, we show that not only is the NMDAR-
601 mediated synaptic component reduced in comparison to the AMPAR currents in the CCK+ cells or
602 PV+ cells, but a similar significant change in seen in anatomically identified PV+ basket cells. The
603 analyses of the quantal miniature currents in identified PV+ basket cells indicate that the reduced
604 NMDAR-to-AMPAR-mediated synaptic responses are due to smaller postsynaptic NMDAR currents,
605 rather than increased AMPAR EPSC. Finally, we show reduced NMDAR-dependent excitatory drive of
606 recurrent GABAergic inhibition in the hippocampus of the NRG1 type-I over-expressing mice utilizing
607 optogenetically-driven selective stimulation of hippocampal pyramidal cells.
608
609 Of note, in this transgenic mouse line the over-expression of NRG1 type-I is under the Thy- 1.2
610 promoter, which is not equally expressed in all hippocampal pyramidal cells (Dobbins et al. 2018).
611 This raises a possibility that NRG1 release in the hippocampus is not homogeneous having variable
612 effects on ErbB4 positive cells. This might at least partially explain the N/A ratio variation in PV+ cells
613 of the NRG1 over-expressing mice illustrated in figure 2. However, the N/A ratio variation may also
614 emerge from lack of the NRG1 receptor in some PV+ cells and CCK+ interneurons (Bean et al., 2014).

615

616 The results suggest that NMDAR-signaling abnormalities in these two major GABAergic interneuron
617 populations may contribute to the hippocampal pathophysiology thought to occur in SZ (Harrison et
618 al., 2003; Gonzalez-Burgos et al., 2011; Curley and Lewis, 2012). In this respect our results bring
619 together three theories of SZ pathophysiology; genetic heritability, inhibitory circuit dysfunction, and
620 NMDAR hypofunction affecting GABAergic inhibitory interneurons such as PV+ basket cells
621 (Zylberman et al., 1995; Lisman et al., 2008; Belforte et al., 2010; Korotkova et al., 2010; Lewis et al.,
622 2011; Gonzalez-Burgos and Lewis, 2012; Volk and Lewis, 2014; Banerjee et al., 2015; Krystal, 2015).
623 Malfunction of PV+ basket cells has been commonly suggested to underlie aberrant co-ordinated
624 network activities, in particular the gamma frequency oscillations, and is associated with cognitive
625 dysfunction in animal models (Cho et al., 2015), and hypothesised to do so as well as in SZ patients
626 (Buonanno, 2010; Uhlhaas and Singer, 2010; Gonzalez-Burgos and Lewis, 2012; Harrison et al., 2012;
627 Marin, 2012; Nakazawa et al., 2012). Interestingly, the specific alterations of gamma oscillation
628 features that were observed in hippocampal slice preparations from the NRG1$^{tg\text{-}type\text{-}I}$ mice (Deakin et
629 al. 2012) differed from findings of *in vivo* studies in which NMDARs were selectively knocked out in
630 PV-expressing interneurons (Korotkova et al., 2010; Carlen et al., 2012). In fact, it has been proposed
631 that NMDAR hypofunction in PV+ cells render the brain networks more prone to exhibit the
632 schizophrenia-associated behavioral and electrophysiological alterations, and that the actual
633 phenotypes develop when NMDAR hypofunction simultaneously co-exists in other neuron types
634 (Bygrave et al., 2016). Importantly, our results here show postsynaptic suppression of the NMDAR
635 signaling in interneurons expressing CCK. In physiological conditions these hippocampal
636 interneurons have large synaptic NMDAR-mediated currents (Fricker and Miles, 2000; Maccaferri
637 and Dingledine, 2002; Matta et al., 2013). Thus, it is likely that the alterations observed in the
638 NRG1$^{tg\text{-}type\text{-}I}$ mouse hippocampal network activity and hippocampus-dependent behavior (Deakin et
639 al. 2009, 2012) emerge at least partially from NMDAR hypofunction in the PV+ and CCK+ interneuron
640 subpopulations. Although we failed to detect changes in AMPAR-mediated glutamatergic currents or

641 in the function of GABAergic synapses, it is possible that these can be subject to changes at a later
642 stage of the phenotype progression also in the NRG1 type-I mutant mice (Woo et al., 2007; Fazzari et
643 al., 2010; Wen et al., 2010; Abe et al., 2011; Ting et al., 2011).
644
645 In summary, our results indicate that synaptic NMDAR-mediated signaling in hippocampal
646 interneurons is sensitive to chronically elevated NRG1 type-I levels. Further studies will be required
647 to determine the mechanism by which NRG1 type-I over-expression results in the observed NMDAR
648 hypofunction, and to what extent these alterations are sufficient to explain the previously reported
649 phenotypes in these mice (Michailov et al, 2004; Deakin et al, 2009, 2012). Possible cellular
650 mechanisms underlying the NMDAR hypofunction include altered receptor subunit phosphorylation
651 (Hahn et al., 2006; Bjarnadottir et al., 2007; Pitcher et al., 2011; Banerjee et al., 2015), or modulation
652 of the trafficking and expression of NMDAR subunits (Ozaki et al., 1997; Gu et al., 2005; Abe et al.,
653 2011; Luo et al., 2014). Importantly it has been shown that neuregulin 2 (NRG2), which also signals
654 via ErbB4, facilitates the physical interaction of ErbB4 with the NMDAR GluN2B subunit leading to
655 internalization of the subunit and hence NMDAR hypofunction (Vullhorst et al. 2015). Finally, the
656 changes in NMDAR-mediated synaptic transmission observed in transgenic NRG1 type-I mice could
657 in part mirror what takes place in SZ, given the elevated NRG1 type-I expression seen in the brain in
658 the disease. Further studies are needed to explore this possibility, and the potential role of
659 therapeutic interventions targeting the NRG1 signaling pathway.
660
661 **References**
662
663 Schizophrenia Working Group of the Psychiatric Genomics Consortium (2014) Biological insights
664 from 108 schizophrenia-associated genetic loci. Nature 511:421-427.

665 Abe Y, Namba H, Kato T, Iwakura Y, Nawa H (2011) Neuregulin-1 signals from the periphery regulate
666 AMPA receptor sensitivity and expression in GABAergic interneurons in developing
667 neocortex. J Neurosci 31:5699-5709.
668 Agarwal A et al. (2014) Dysregulated expression of neuregulin-1 by cortical pyramidal neurons
669 disrupts synaptic plasticity. Cell Rep 8:1130-1145.
670 Armstrong C, Soltesz I (2012) Basket cell dichotomy in microcircuit function. J Physiol 590:683-694.
671 Banerjee A, Wang HY, Borgmann-Winter KE, MacDonald ML, Kaprielian H, Stucky A, Kvasic J, Egbujo
672 C, Ray R, Talbot K, Hemby SE, Siegel SJ, Arnold SE, Sleiman P, Chang X, Hakonarson H, Gur RE,
673 Hahn CG (2015) Src kinase as a mediator of convergent molecular abnormalities leading to
674 NMDAR hypoactivity in schizophrenia. Mol Psychiatry 20:1091-1100.
675 Bean JC, Lin TW, Sathyamurthy A, Liu F, Yin DM, Xiong WC, Mei L (2014) Genetic labeling reveals
676 novel cellular targets of schizophrenia susceptibility gene: distribution of GABA and non-
677 GABA ErbB4-positive cells in adult mouse brain. J Neurosci 34:13549-13566.
678 Belforte JE, Zsiros V, Sklar ER, Jiang Z, Yu G, Li Y, Quinlan EM, Nakazawa K (2010) Postnatal NMDA
679 receptor ablation in corticolimbic interneurons confers schizophrenia-like phenotypes. Nat
680 Neurosci 13:76-83.
681 Bjarnadottir M, Misner DL, Haverfield-Gross S, Bruun S, Helgason VG, Stefansson H, Sigmundsson A,
682 Firth DR, Nielsen B, Stefansdottir R, Novak TJ, Stefansson K, Gurney ME, Andresson T (2007)
683 Neuregulin1 (NRG1) signaling through Fyn modulates NMDA receptor phosphorylation:
684 differential synaptic function in NRG1+/- knock-outs compared with wild-type mice. J
685 Neurosci 27:4519-4529.
686 Bocchio M, Fucsina G, Oikonomidis L, McHugh SB, Bannerman DM, Sharp T, Capogna M (2015)
687 Increased serotonin transporter expression reduces fear and recruitment of parvalbumin
688 interneurons of the amygdala. Neuropsychopharmacology 40:3015-3026.

689 Bodor AL, Katona I, Nyiri G, Mackie K, Ledent C, Hajos N, Freund TF (2005) Endocannabinoid signaling
690 in rat somatosensory cortex: laminar differences and involvement of specific interneuron
691 types. J Neurosci 25:6845-6856.
692 Boer S, Berk M, Dean B (2009) Levels of neuregulin 1 and 3 proteins in Brodmann's area 46 from
693 subjects with schizophrenia and bipolar disorder. Neurosci Lett 466:27-29.
694 Brown JA, Horvath S, Garbett KA, Schmidt MJ, Everheart M, Gellert L, Ebert P, Mirnics K (2014) The
695 role of cannabinoid 1 receptor expressing interneurons in behavior. Neurobiol Dis 63:210-
696 221.
697 Buonanno A (2010) The neuregulin signaling pathway and schizophrenia: from genes to synapses
698 and neural circuits. Brain Res Bull 83:122-131.
699 Burgunder JM, Young WS (1990) Cortical neurons expressing the cholecystokinin gene in the rat:
700 distribution in the adult brain, ontogeny, and some of their projections J Comp Neurol.
701 1:300(1):26-46.
702 Buzsaki G, Wang XJ (2012) Mechanisms of gamma oscillations. Annu Rev Neurosci 35:203-225.
703 Bygrave AM, Masiulis S, Nicholson E, Berkemann M, Barkus C, Sprengel R, Harrison PJ, Kullmann DM,
704 Bannerman DM, Katzel D (2016) Knockout of NMDA-receptors from parvalbumin
705 interneurons sensitizes to schizophrenia-related deficits induced by MK-801. Transl
706 Psychiatry 6:e778.
707 Campanac E, Gasselin C, Baude A, Rama S, Ankri N, Debanne D (2013) Enhanced intrinsic excitability
708 in basket cells maintains excitatory-inhibitory balance in hippocampal circuits. Neuron
709 77:712-722.
710 Carlen M, Meletis K, Siegle JH, Cardin JA, Futai K, Vierling-Claassen D, Ruhlmann C, Jones SR,
711 Deisseroth K, Sheng M, Moore CI, Tsai LH (2012) A critical role for NMDA receptors in
712 parvalbumin interneurons for gamma rhythm induction and behavior. Mol Psychiatry
713 17:537-548.

714 Chen YJ, Johnson MA, Lieberman MD, Goodchild RE, Schobel S, Lewandowski N, Rosoklija G, Liu RC,
715 Gingrich JA, Small S, Moore H, Dwork AJ, Talmage DA, Role LW (2008) Type III neuregulin-1 is
716 required for normal sensorimotor gating, memory-related behaviors, and corticostriatal
717 circuit components. J Neurosci 28:6872-6883.
718 Chen YJ, Zhang M, Yin DM, Wen L, Ting A, Wang P, Lu YS, Zhu XH, Li SJ, Wu CY, Wang XM, Lai C, Xiong
719 WC, Mei L, Gao TM (2010) ErbB4 in parvalbumin-positive interneurons is critical for
720 neuregulin 1 regulation of long-term potentiation. Proc Natl Acad Sci U S A 107:21818-
721 21823.
722 Cho KK, Hoch R, Lee AT, Patel T, Rubenstein JL, Sohal VS (2015) Gamma rhythms link prefrontal
723 interneuron dysfunction with cognitive inflexibility in Dlx5/6(+/-) mice. Neuron 85:1332-
724 1343.
725 Chong VZ, Thompson M, Beltaifa S, Webster MJ, Law AJ, Weickert CS (2008) Elevated neuregulin-1
726 and ErbB4 protein in the prefrontal cortex of schizophrenic patients. Schizophrenia research
727 100:270-280.
728 Cobb SR, Buhl EH, Halasy K, Paulsen O, Somogyi P (1995) Synchronization of neuronal activity in
729 hippocampus by individual GABAergic interneurons. Nature 378:75-78.
730 Corfas G, Roy K, Buxbaum JD (2004) Neuregulin 1-erbB signaling and the molecular/cellular basis of
731 schizophrenia. Nat Neurosci 7:575-580.
732 Coyle JT (2012) NMDA receptor and schizophrenia: a brief history. Schizophr Bull 38:920-926.
733 Curley AA, Lewis DA (2012) Cortical basket cell dysfunction in schizophrenia. J Physiol 590:715-724.
734 Deakin IH, Law AJ, Oliver PL, Schwab MH, Nave KA, Harrison PJ, Bannerman DM (2009) Behavioural
735 characterization of neuregulin 1 type I overexpressing transgenic mice. Neuroreport
736 20:1523-1528.
737 Deakin IH, Nissen W, Law AJ, Lane T, Kanso R, Schwab MH, Nave KA, Lamsa KP, Paulsen O,
738 Bannerman DM, Harrison PJ (2012) Transgenic overexpression of the type I isoform of

neuregulin 1 affects working memory and hippocampal oscillations but not long-term potentiation. Cereb Cortex 22:1520-1529.

Del Pino I, Brotons-Mas JR, Marques-Smith A, Marighetto A, Frick A, Marin O, Rico B (2017) Abnormal wiring of CCK+ basket cells disrupts spatial information coding. Nature Neurosci 20:784-792.

Deleuze C, Huguenard JR (2016) Two classes of excitatory synaptic responses in rat thalamic reticular neurons. J Neurophysiol 116:995-1011.

Dobbins DL, Klorig DC, Smith T, Godwin DW (2018) Expression of channelrhodopsin-2 localized within the deep CA1 hippocampal sublayer in the Thy1 line 18 mouse. Brain Res. 15;1679:179-184.

Ellender TJ, Paulsen O (2010) The many tunes of perisomatic targeting interneurons in the hippocampal network. Front Cell Neurosci 4:26.

Fasano C, Rocchetti J, Pietrajtis K, Zander JF, Manseau F, Sakae DY, Marcus-Sells M, Ramet L, Morel LJ, Carrel D, Dumas S, Bolte S, Bernard V, Vigneault E, Goutagny R, Ahnert-Hilger G, Giros B, Daumas S, Williams S, El Mestikawy S (2017) Regulation of the Hippocampal Network by VGLUT3-Positive CCK- GABAergic Basket Cells. Front Cell Neurosci 11:140.

Fazzari P, Paternain AV, Valiente M, Pla R, Lujan R, Lloyd K, Lerma J, Marin O, Rico B (2010) Control of cortical GABA circuitry development by Nrg1 and ErbB4 signalling. Nature 464:1376-1380.

Flames N, Long JE, Garratt AN, Fischer TM, Gassmann M, Birchmeier C, Lai C, Rubenstein JL, Marin O (2004) Short- and long-range attraction of cortical GABAergic interneurons by neuregulin-1. Neuron 44:251-261.

Fricker D, Miles R (2000) EPSP amplification and the precision of spike timing in hippocampal neurons. Neuron 28:559-569.

Geibel M, Badurek S, Horn JM, Vatanashevanopakorn C, Koudelka J, Wunderlich CM, Bronneke HS, Wunderlich FT, Minichiello L (2014) Ablation of TrkB signalling in CCK neurons results in hypercortisolism and obesity. Nat Commun 5:3427.

765 Gilmour G, Dix S, Fellini L, Gastambide F, Plath N, Steckler T, Talpos J, Tricklebank M (2012) NMDA
766 receptors, cognition and schizophrenia--testing the validity of the NMDA receptor
767 hypofunction hypothesis. Neuropharmacology 62:1401-1412.
768 Gonzalez-Burgos G, Lewis DA (2012) NMDA receptor hypofunction, parvalbumin-positive neurons,
769 and cortical gamma oscillations in schizophrenia. Schizophr Bull 38:950-957.
770 Gonzalez-Burgos G, Fish KN, Lewis DA (2011) GABA neuron alterations, cortical circuit dysfunction
771 and cognitive deficits in schizophrenia. Neural Plast 2011:723184.
772 Gonzalez-Burgos G, Cho RY, Lewis DA (2015) Alterations in cortical network oscillations and
773 parvalbumin neurons in schizophrenia. Biol Psychiatry 77:1031-1040.
774 Gu Z, Jiang Q, Fu AK, Ip NY, Yan Z (2005) Regulation of NMDA receptors by neuregulin signaling in
775 prefrontal cortex. J Neurosci 25:4974-4984.
776 Hahn CG (2011) A Src link in schizophrenia. Nat Med 17:425-427.
777 Hahn CG, Wang HY, Cho DS, Talbot K, Gur RE, Berrettini WH, Bakshi K, Kamins J, Borgmann-Winter
778 KE, Siegel SJ, Gallop RJ, Arnold SE (2006) Altered neuregulin 1-erbB4 signaling contributes to
779 NMDA receptor hypofunction in schizophrenia. Nat Med 12:824-828.
780 Hall J, Trent S, Thomas KL, O'Donovan MC, Owen MJ (2015) Genetic risk for schizophrenia:
781 convergence on synaptic pathways involved in plasticity. Biol Psychiatry 77:52-58.
782 Harrison PJ, Weinberger DR (2005) Schizophrenia genes, gene expression, and neuropathology: on
783 the matter of their convergence. Mol Psychiatry 10:40-68; image 45.
784 Harrison PJ, Law AJ, Eastwood SL (2003) Glutamate receptors and transporters in the hippocampus
785 in schizophrenia. Ann N Y Acad Sci 1003:94-101.
786 Harrison PJ, Pritchett D, Stumpenhorst K, Betts JF, Nissen W, Schweimer J, Lane T, Burnet PW, Lamsa
787 KP, Sharp T, Bannerman DM, Tunbridge EM (2012) Genetic mouse models relevant to
788 schizophrenia: taking stock and looking forward. Neuropharmacology 62:1164-1167.

789 Hashimoto R, Straub RE, Weickert CS, Hyde TM, Kleinman JE, Weinberger DR (2004) Expression
790 analysis of neuregulin-1 in the dorsolateral prefrontal cortex in schizophrenia. Mol
791 Psychiatry 9:299-307.
792 Huang Y, Yoon K, Ko H, Jiao S, Ito W, Wu JY, Yung WH, Lu B, Morozov A (2016) 5-HT3a receptors
793 modulate hippocampal gamma oscillations by regulating synchrony of parvalbumin-positive
794 interneurons. Cereb Cortex 26:576-585.
795 Kato T, Abe Y, Sotoyama H, Kakita A, Kominami R, Hirokawa S, Ozaki M, Takahashi H, Nawa H (2011)
796 Transient exposure of neonatal mice to neuregulin-1 results in hyperdopaminergic states in
797 adulthood: implication in neurodevelopmental hypothesis for schizophrenia. Mol Psychiatry
798 16:307-320.
799 Katona I, Sperlagh B, Sik A, Kafalvi A, Vizi ES, Mackie K, Freund TF (1999) Presynaptically located CB1
800 cannabinoid receptors regulate GABA release from axon terminals of specific hippocampal
801 interneurons. J Neurosci 19:4544-4558.
802 Klausberger T, Somogyi P (2008) Neuronal diversity and temporal dynamics: the unity of
803 hippocampal circuit operations. Science 321:53-57.
804 Korotkova T, Fuchs EC, Ponomarenko A, von Engelhardt J, Monyer H (2010) NMDA receptor ablation
805 on parvalbumin-positive interneurons impairs hippocampal synchrony, spatial
806 representations, and working memory. Neuron 68:557-569.
807 Krivosheya D, Tapia L, Levinson JN, Huang K, Kang Y, Hines R, Ting AK, Craig AM, Mei L, Bamji SX, El-
808 Husseini A (2008) ErbB4-neuregulin signaling modulates synapse development and dendritic
809 arborization through distinct mechanisms. J Biol Chem 283:32944-32956.
810 Krystal JH (2015) Deconstructing N-methyl-d-aspartate glutamate receptor contributions to cortical
811 circuit functions to construct better hypotheses about the pathophysiology of schizophrenia.
812 Biol Psychiatry 77:508-510.
813 Kullmann DM, Lamsa KP (2011) LTP and LTD in cortical GABAergic interneurons: emerging rules and
814 roles. Neuropharmacology 60:712-719.

815 Lasztoczi B, Tukker JJ, Somogyi P, Klausberger T (2011) Terminal field and firing selectivity of
816 cholecystokinin-expressing interneurons in the hippocampal CA3 area. J Neurosci 31:18073-
817 18093.
818 Law AJ, Lipska BK, Weickert CS, Hyde TM, Straub RE, Hashimoto R, Harrison PJ, Kleinman JE,
819 Weinberger DR (2006) Neuregulin 1 transcripts are differentially expressed in schizophrenia
820 and regulated by 5' SNPs associated with the disease. Proc Natl Acad Sci U S A 103:6747-
821 6752.
822 Lewis DA, Fish KN, Arion D, Gonzalez-Burgos G (2011) Perisomatic inhibition and cortical circuit
823 dysfunction in schizophrenia. Curr Opin Neurobiol 21:866-872.
824 Li H, Chou SJ, Hamasaki T, Perez-Garcia CG, O'Leary DD (2012a) Neuregulin repellent signaling via
825 ErbB4 restricts GABAergic interneurons to migratory paths from ganglionic eminence to
826 cortical destinations. Neural Dev 7:10.
827 Li KX, Lu YM, Xu ZH, Zhang J, Zhu JM, Zhang JM, Cao SX, Chen XJ, Chen Z, Luo JH, Duan S, Li XM
828 (2012b) Neuregulin 1 regulates excitability of fast-spiking neurons through Kv1.1 and acts in
829 epilepsy. Nat Neurosci 15:267-273.
830 Liu Y, Tao YM, Woo RS, Xiong WC, Mei L (2007) Stimulated ErbB4 internalization is necessary for
831 neuregulin signaling in neurons. Biochem Biophys Res Commun. 9;354(2):505-10.
832 Lisman JE, Coyle JT, Green RW, Javitt DC, Benes FM, Heckers S, Grace AA (2008) Circuit-based
833 framework for understanding neurotransmitter and risk gene interactions in schizophrenia.
834 Trends Neurosci 31:234-242.
835 Longart M, Chatani-Hinze M, Gonzalez CM, Vullhorst D, Buonanno A (2007) Regulation of ErbB-4
836 endocytosis by neuregulin in GABAergic hippocampal interneurons. Brain Res Bull 73:210-
837 219.
838 Lopez-Bendito G, Cautinat A, Sanchez JA, Bielle F, Flames N, Garratt AN, Talmage DA, Role LW,
839 Charnay P, Marin O, Garel S (2006) Tangential neuronal migration controls axon guidance: a
840 role for neuregulin-1 in thalamocortical axon navigation. Cell 125:127-142.

841 Luo X, He W, Hu X, Yan R (2014) Reversible overexpression of bace1-cleaved neuregulin-1 N-terminal
842 fragment induces schizophrenia-like phenotypes in mice. Biol Psychiatry 76:120-127.
843 Maccaferri G, McBain CJ (1995) Passive propagation of LTD to stratum oriens-alveus inhibitory
844 neurons modulates the temporoammonic input to the hippocampal CA1 region. Neuron
845 15:137-145.
846 Maccaferri G, Dingledine R (2002) Control of feedforward dendritic inhibition by NMDA receptor-
847 dependent spike timing in hippocampal interneurons. J Neurosci 22:5462-5472.
848 Manseau F, Marinelli S, Mendez P, Schwaller B, Prince DA, Huguenard JR, Bacci A (2010)
849 Desynchronization of neocortical networks by asynchronous release of GABA at autaptic and
850 synaptic contacts from fast-spiking interneurons. PLoS Biol 8: e1000492.
851 Marin O (2012) Interneuron dysfunction in psychiatric disorders. Nat Rev Neurosci 13:107-120.
852 Matta JA, Pelkey KA, Craig MT, Chittajallu R, Jeffries BW, McBain CJ (2013) Developmental origin
853 dictates interneuron AMPA and NMDA receptor subunit composition and plasticity. Nat
854 Neurosci 16:1032-1041.
855 Medrihan L, Sagi Y, Inde Z, Krupa O, Daniels C, Peyrache A, Greengard P (2017) Initiation of
856 behavioral response to antidepressants by cholecystokinin neurons of the dentate gyrus.
857 Neuron 95:564-576.
858 Michailov GV, Sereda MW, Brinkmann BG, Fischer TM, Haug B, Birchmeier C, Role L, Lai C, Schwab
859 MH, Nave KA (2004) Axonal neuregulin-1 regulates myelin sheath thickness. Science
860 304:700-703.
861 Morino P, Herrera-Marschitz M, Castel MN, Ungerstedt U, Varro A, Dockray G, Hökfelt T (1994)
862 Cholecystokinin in cortico-striatal neurons in the rat: immunohistochemical studies at the
863 light and electron microscopical level. Eur J Neurosci 6:681-692.
864 Nakazawa K, Zsiros V, Jiang Z, Nakao K, Kolata S, Zhang S, Belforte JE (2012) GABAergic interneuron
865 origin of schizophrenia pathophysiology. Neuropharmacology 62:1574-1583.

866 Neddens J, Buonanno A (2010) Selective populations of hippocampal interneurons express ErbB4
867 and their number and distribution is altered in ErbB4 knockout mice. Hippocampus 20:724-
868 744.
869 Neddens J, Fish KN, Tricoire L, Vullhorst D, Shamir A, Chung W, Lewis DA, McBain CJ, Buonanno A
870 (2011) Conserved interneuron-specific ErbB4 expression in frontal cortex of rodents,
871 monkeys, and humans: implications for schizophrenia. Biol Psychiatry 70:636-645.
872 Nissen W, Szabo A, Somogyi J, Somogyi P, Lamsa KP (2010) Cell type-specific long-term plasticity at
873 glutamatergic synapses onto hippocampal interneurons expressing either parvalbumin or
874 CB1 cannabinoid receptor. J Neurosci 30:1337-1347.
875 Okada M, Corfas G (2004) Neuregulin1 downregulates postsynaptic GABAA receptors at the
876 hippocampal inhibitory synapse. Hippocampus 14:337-344.
877 Olney JW, Farber NB (1995) Glutamate receptor dysfunction and schizophrenia. Arch Gen Psychiatry
878 52:998-1007.
879 Ozaki M, Sasner M, Yano R, Lu HS, Buonanno A (1997) Neuregulin-beta induces expression of an
880 NMDA-receptor subunit. Nature 390:691-694.
881 Papp OI, Karlocai MR, Toth IE, Freund TF, Hajos N (2013) Different input and output properties
882 characterize parvalbumin-positive basket and axo-axonic cells in the hippocampal CA3
883 subfield. Hippocampus 23:903-918.
884 Parlapani E, Schmitt A, Wirths O, Bauer M, Sommer C, Rueb U, Skowronek MH, Treutlein J, Petroianu
885 GA, Rietschel M, Falkai P (2010) Gene expression of neuregulin-1 isoforms in different brain
886 regions of elderly schizophrenia patients. World J Biol Psychiatry 11:243-250.
887 Pelkey KA, Chittajallu R, Craig MT, Tricoire L, Wester JC, McBain CJ (2017) Hippocampal GABAergic
888 Inhibitory Interneurons. Physiol Rev 97:1619-1747.
889 Perez Y, Morin F, Lacaille JC (2001) A hebbian form of long-term potentiation dependent on
890 mGluR1a in hippocampal inhibitory interneurons. Proc Natl Acad Sci U S A 98:9401-9406.

Pitcher GM, Kalia LV, Ng D, Goodfellow NM, Yee KT, Lambe EK, Salter MW (2011) Schizophrenia susceptibility pathway neuregulin 1-ErbB4 suppresses Src upregulation of NMDA receptors. Nat Med 17:470-478.

Rombo DM, Newton K, Nissen W, Badurek S, Horn JM, Minichiello L, Jefferys JG, Sebastiao AM, Lamsa KP (2015) Synaptic mechanisms of adenosine A2A receptor-mediated hyperexcitability in the hippocampus. Hippocampus 25(5):566-80.

Schmidt MJ, Mirnics K (2015) Neurodevelopment, GABA system dysfunction, and schizophrenia. Neuropsychopharmacology 40:190-206.

Schmidt MJ, Horvath S, Ebert P, Norris JL, Seeley EH, Brown J, Gellert L, Everheart M, Garbett KA, Grice TW, Caprioli RM, Mirnics K (2014) Modulation of behavioral networks by selective interneuronal inactivation. Mol Psychiatry 19:580-587.

Stefansson H et al. (2002) Neuregulin 1 and susceptibility to schizophrenia. Am J Hum Genet 71:877-892.

Ting AK, Chen Y, Wen L, Yin DM, Shen C, Tao Y, Liu X, Xiong WC, Mei L (2011) Neuregulin 1 promotes excitatory synapse development and function in GABAergic interneurons. J Neurosci 31:15-25.

Tsou K, Mackie K, Sanudo-Pena MC, Walker JM (1999) Cannabinoid CB1 receptors are localized primarily on cholecystokinin-containing GABAergic interneurons in the rat hippocampal formation. Neuroscience 93:969-975.

Uhlhaas PJ, Singer W (2010) Abnormal neural oscillations and synchrony in schizophrenia. Nat Rev Neurosci 11:100-113.

Vargish GA, Pelkey KA, Yuan X, Chittajallu R, Collins D, Fang C, McBain CJ (2017) Persistent inhibitory circuit defects and disrupted social behaviour following in utero exogenous cannabinoid exposure. Mol Psychiatry 22:56-67.

Volk DW, Lewis DA (2014) Early developmental disturbances of cortical inhibitory neurons: contribution to cognitive deficits in schizophrenia. Schizophr Bull 40:952-957.

917 Vullhorst D, Neddens J, Karavanova I, Tricoire L, Petralia RS, McBain CJ, Buonanno A (2009) Selective
918 expression of ErbB4 in interneurons, but not pyramidal cells, of the rodent hippocampus. J
919 Neurosci 29:12255-12264.
920 Vullhorst D, Mitchell RM, Keating C, Roychowdhury S, Karavanova I, Tao-Cheng JH, Buonanno A
921 (2015) A negative feedback loop controls NMDA receptor function in cortical interneurons
922 via neuregulin 2/ErbB4 signalling. Nat Commun 6:7222.
923 Weickert CS, Tiwari Y, Schofield PR, Mowry BJ, Fullerton JM (2012) Schizophrenia-associated HapICE
924 haplotype is associated with increased NRG1 type III expression and high nucleotide
925 diversity. Transl Psychiatry 2:e104.
926 Weickert CS, Fung SJ, Catts VS, Schofield PR, Allen KM, Moore LT, Newell KA, Pellen D, Huang XF,
927 Catts SV, Weickert TW (2013) Molecular evidence of N-methyl-D-aspartate receptor
928 hypofunction in schizophrenia. Mol Psychiatry 18:1185-1192.
929 Wen L, Lu YS, Zhu XH, Li XM, Woo RS, Chen YJ, Yin DM, Lai C, Terry AV, Jr., Vazdarjanova A, Xiong
930 WC, Mei L (2010) Neuregulin 1 regulates pyramidal neuron activity via ErbB4 in parvalbumin-
931 positive interneurons. Proc Natl Acad Sci U S A 107:1211-1216.
932 Woo RS, Li XM, Tao Y, Carpenter-Hyland E, Huang YZ, Weber J, Neiswender H, Dong XP, Wu J,
933 Gassmann M, Lai C, Xiong WC, Gao TM, Mei L (2007) Neuregulin-1 enhances depolarization-
934 induced GABA release. Neuron 54:599-610.
935 Yau HJ, Wang HF, Lai C, Liu FC (2003) Neural development of the neuregulin receptor ErbB4 in the
936 cerebral cortex and the hippocampus: preferential expression by interneurons tangentially
937 migrating from the ganglionic eminences. Cereb Cortex 13:252-264.
938 Yin DM, Chen YJ, Lu YS, Bean JC, Sathyamurthy A, Shen C, Liu X, Lin TW, Smith CA, Xiong WC, Mei L
939 (2013) Reversal of behavioral deficits and synaptic dysfunction in mice overexpressing
940 neuregulin 1. Neuron 78:644-657.
941 Zylberman I, Javitt DC, Zukin SR (1995) Pharmacological augmentation of NMDA receptor function
942 for treatment of schizophrenia. Ann N Y Acad Sci 757:487-491.

943

944 **Figure legends**

945

946 **Figure 1. ErbB4 expression in PV+ and PV- interneurons and the ErbB4 expression levels in**
947 **hippocampus of wild-type and the NRG1$^{tg\text{-}type\text{-}I}$ mice**

948 ***A,*** Immunostaining for ErbB4, the NRG1 receptor, in the ventral hippocampus CA3 area neurons
949 using highly specific rabbit anti-ErbB4 (polyclonal anti-antiserum 5941) (Neddens and Buonanno,
950 2010).

951 *(A1)* Double immunolabeling for PV (Cy3) and ErbB4 (Alexa488). Merged image shows double-
952 labeled neurons (arrowhead) and ErbB4+ interneurons immunonegative for PV (arrows). *s.r*, *stratum*
953 *radiatum. (A2)* In mice with genetic fluorescence marker (tdTomato) in CCK cells (tdTom-CCK), ErbB4
954 immunostaining in Alexa488 shows the expression in many CCK+ neurons in *stratum radiatum (s.r.)*
955 and *pyramidale (s.p.)*. Cre-dependent tdTomato signal is strong in putative CA3 interneurons (soma
956 in *s.r.*) and weaker in *stratum pyramidale* where majority of pyramidal cell somata are located
957 (contrast adjustment in the image). In merged image arrowheads point at interneuron somata with
958 both fluorescent signals. Scale bars 50 µm. Confocal microscope images.

959 ***B-D***, Cell density analysis of hippocampal interneurons immunopositive for ErbB4 in the wild-type
960 (WT) and in the NRG1 type-I over-expressing mice (NRG1$^{tg\text{-}type\text{-}I}$ mice).

961 *B1)* ErbB4 immunoreaction (20 µm stack image) in sample hippocampal sections of a WT (left) and a
962 NRG1$^{tg\text{-}type\text{-}I}$ mice (right). Scale bar 100 µm.

963 *B2)* Box plots show ErbB4+ cell soma density (measured to 20 µm depth from the section surface) in
964 the WT (blue, n = 9 sections in 3 mice) and the NRG1$^{tg\text{-}type\text{-}I}$ mice (red, 12 sections in 3 mice)
965 hippocampi. The plot shows median and interquartile range. Fewer ErbB4+ somata were detected in
966 the NRG1$^{tg\text{-}type\text{-}I}$ mice compared to the WT mice in all hippocampal areas. From the left: whole
967 hippocampus including areas CA1, CA2 and CA3; area CA1-2 restricted to *alveus, stratum oriens* and
968 *stratum pyramidale*; area CA1-2 restricted to *stratum radiatum and lacunosum-moleculare*; area CA3

containing *alveus* with *strata oriens* and *pyramidale*; and area CA3 with *strata lucidum* and *radiatum* and *lacunosum-moleculare*. *p* -values compare data between genotypes (Mann-Whitney U-test). *C1)* Immunoreaction for PV in the same sections as in B1. *C2)* Cell density analyses show no difference in the observed PV+ cell somata between the two genotypes as indicated by *p* values (Mann-Whitney U-test). Box plots as in B2. *D1)* Merged ErbB4 and PV immunolabeling in the sample sections above. *D2)* Box plots show proportion of the double-labeled cells (co-immunoreactive for ErbB4 and PV) in the PV+ cell population in WT and NRG1$^{tg\text{-}type\text{-}I}$ mice. The analyses show unaltered proportion in the whole hippocampus and in most sub-regions compared separately. The significant *p* value is bolded. ***E,*** Immunoblot analysis of ErbB4 expression levels in WT and in NRG1$^{tg\text{-}type\text{-}I}$ mice using hippocampal extracts. *E1)* The antibody against ErbB4 detects a band of the predicted protein size (~150 kDa) in hippocampal protein extracts. Left lane: No non-specific bands were detected in the secondary-only antibody control (right lane). *E2)* Hippocampal extracts from 6 WT and 6 NRG1$^{tg\text{-}type\text{-}I}$ mice of both genders (3 males and 3 females in each genotype in scrambled order) tested for ErbB4 expression. GAPDH was used as a loading control. *E3)* Box plot shows (mean and interquartile range) densitometry analysis comparison of the ErbB4 levels normalized by the GAPDH in the 12 hippocampal extracts (6 in both genotypes including 3 males and 3 females). The results indicate a general trend to lower ErbB4 levels in NRG1$^{tg\text{-}type\text{-}I}$ mice, but with no significant difference between the genotypes (Mann-Whitney U-test).

Figure 2. Reduced synaptic NMDAR-mediated currents in hippocampal interneurons expressing PV or CCK in the NRG1$^{tg\text{-}type\text{-}I}$ mice

A, Interneurons expressing PV or CCK in the CA3 area. *A1)* Sample image of a recorded PV interneuron identified by PV expression-dependent fluorescent genetic marker tdTomato (tdTom-PV). Recorded cells were also visualized with filled neurobiotin (nb, Alexa488). *A2)* Recorded cells not showing tdTomato signal were identified as CCK interneurons *post hoc* with (*left*) positive

995 somatic immunoreaction for pro-CCK (Cy5, arrow head) or in the absence of recovered soma and
996 dendrites, (*right)* by positive reaction for axonal cannabinoid receptor type 1 (CB1R, Cy3). Scale bars
997 from left; 10, 20 and 10 µm, respectively.
998 ***B,*** Reduced NMDAR- versus AMPAR -mediated EPSCs ratio (N/A ratio) in glutamatergic synaptic
999 input to interneurons expressing PV. Electrical stimulation was applied in CA3 *stratum oriens* aiming
1000 to activate associative/commissural pathways. AMPAR-mediated EPSCs were recorded at -60 mV (in
1001 PiTX, 100 µM), and blocked by NBQX (25 µM) to record NMDAR-mediated EPSCs (at +40 mV from
1002 their reversal potential). *B1)* Averaged EPSCs (10 traces) in sample PV+ interneurons in from WT and
1003 NRG1$^{tg\text{-}type\text{-}I}$ mouse (black, AMPAR EPSCs*;* green, NMDAR EPSCs in the presence of NBQX*;* gray,
1004 following application of NMDAR blocker DL-AP5. Scale bars 100 pA, 25 ms. *B2*) Cumulative
1005 histograms of the N/A amplitude ratios in all studied PV+ interneurons (WT, blue line and NRG1$^{tg\text{-}type\text{-}I}$
1006 mice, red line). *p* indicates difference between the genotypes (Mann-Whitney U-test).
1007 ***C,*** Reduced N/A ratio in glutamatergic synaptic input to the CCK+ interneurons. *C1)* Averaged EPSCs
1008 (10) in sample cells in the WT and in the NRG1$^{tg\text{-}type\text{-}I}$ mouse with scaling as above. *C2)* Cumulative
1009 histogram quantifying the N/A ratios in CCK interneurons with *p* indicating significant difference
1010 between the genotypes (Mann-Whitney U-test).
1011 ***D,*** The N/A ratio is unaltered between the genotypes in the CA3 pyramidal cells. *D1)* Averaged EPSCs
1012 (10 traces) in sample pyramidal cells with scaling as above. *D2)* Cumulative histograms of the N/A
1013 ratios.
1014
1015 **Figure 3. Reduced synaptic NMDAR-mediated currents in identified PV basket cells in the NRG1$^{tg\text{-}}$**
1016 **$^{type\text{-}I}$ mice**
1017 Identified PV basket cells (PVBCs) in the recorded interneuron population (see figure 2) show
1018 reduced N/A -ratio in the NRG1$^{tg\text{-}type\text{-}I}$ mice.
1019 ***A,*** Illustration of a sample PVBC (70 µm-thick section) in WT (axon blue, soma and dendrites red; s.r.,
1020 *stratum radiatum*; s.luc., *lucidum*; s.p., *pyramidale*; s.o., *oriens*). Scale 100 µm.

B, The N/A -EPSC amplitude ratio in identified basket cells. *B1)* Averaged (10) EPSCs in a PVBC from WT and NRG1$^{tg\text{-}type\text{-}I}$ mouse. Black, AMPAR EPSCs at -60 mV*;* green EPSCs (at +40 mV from their reversal potential in the presence of NBQX, 25 µM); grey EPSCs are following the application of DL-AP5 (100 µM). PiTX (100 µM) was present in all experiments. Scale bars 50 pA, 25 ms. *B2)* Plot shows N/A ratio of every identified PVBC in the wild-type (WT, blue circles) and in the NRG1$^{tg\text{-}type\text{-}I}$ mice (red circles), and their mean ± s.e.m. (n = 10 and 10 cells). *p* value indicates highly significant difference (*t*-test).

Figure 4. Quantal current analysis in parvalbumin basket cells shows unaltered AMPAR mEPSCs in the NRG1$^{tg\text{-}type\text{-}I}$ mice

A, Recording of miniature AMPAR- and NMDAR-mediated EPSCs (mEPSCs) in identified CA3 area PVBCs (in the presence of TTX 1 µM and PiTX 100 µM). *A1)* Illustration of a recorded and partially reconstructed PVBC (70 µm thick section) in WT mouse. Scale 100 µm. *A2)* AMPAR mEPSCs in a PVBC in the WT mouse (at -65 mV). *Left:* The mEPSCs shown in 45 s time window. *Right:* Six events superimposed in 15 ms time window. *A3)* AMPAR mEPSCs in a PVBC in the NRG1$^{tg\text{-}type\text{-}I}$ mouse. *A4)* NMDAR mEPSCs in the same wild-type mouse PVBC as in A2 after blockade of AMPARs by NBQX (25 µM, recorded at +40 mV). *Left:* The mEPSCs shown in 45 s time window. *Middle:* The mEPSCs blockade with DL-AP5 (100 µM, application indicated by horizontal bar). *Right:* Six superimposed mEPSCs in 80 ms time window. *A5)* NMDAR mEPSCs blocked by DL-AP5 in NRG1$^{tg\text{-}type\text{-}I}$ mouse PVBC shown in A3. *A6)* Box plot (median, interquartile range) summarizes AMPAR- and NMDAR- mEPSC frequency (measured at least 3 min) in PVBC in WT (blue) and NRG1$^{tg\text{-}type\text{-}I}$ mice (red). *A7)* Box plot summarizes mEPSC amplitude. Note moderately but significantly smaller NMDAR mEPSC in the NRG1$^{tg\text{-}type\text{-}I}$ mice PVBCs (Mann-Whitney U-test). The significant *p* value is bolded.

B, Unaltered NMDAR- and AMPAR-mediated mEPSCs in the CA3 area pyramidal cells in NRG1$^{tg\text{-}type\text{-}I}$ mice. *B1-2)* Sample traces showing AMPAR mEPSCs in pyramidal cells of both genotypes. *B3-4)* Respectively, NMDAR EPSCs in the same cells. *B5)* Box plot (median, interquartile range)

summarizing the AMPAR- and the NMDAR-mediated mEPSC frequency (WT blue, NRG1$^{tg\text{-}type\text{-}I}$ mice red). *B6)* Summary of he AMPAR- and the NMDAR- mEPSC amplitudes in the two genotypes (Mann-Whitney U-test).

Figure 5. GABAergic synaptic transmission from either PV+ or CCK+ cells is not significantly altered in NRG1$^{tg\text{-}type\text{-}I}$ mice

A, Experimental design showing optogenetic stimulation (at 473 nm laser spot, 20 µm diameter) of GABAergic fibres in the CA3 *stratum pyramidale* in slices from ChR2-eYFP-transfected mice expressing Cre-protein either in PV+ cells (*A1*) or CCK+ cells (*A2*). *Left:* Schematic illustration of the experiment with whole-cell recording in CA3 PCs and optogenetic stimulation focused on *stratum pyramidale (s.p.)*. *Right:* Confocal microscope images from sample slices (visualised *post hoc*) showing eYFP fluorescence (green) in the PV- (above) or the CCK-Cre mice. Postsynaptic neurobiotin-filled pyramidal cells are shown red with an inset of a spiny pyramidal cell apical dendrite. Scale 50 µm.

B, Sample experiment showing optogenetically evoked GABAergic IPSCs in a postsynaptic pyramidal cell using minimal stimulation. Monosynaptic IPSCs (black circles) were evoked by smallest stimulation power eliciting IPSCs in the PC. Open circles: failures; red circles: additional IPSCs elicited by increased stimulation power. Timing of laser pulses with representative IPSCs in the experiment is shown above.

C, The optogenetically evoked GABAergic IPSCs from PV cell fibers do not differ significantly between WT mice (blue) and NRG1$^{tg\text{-}type\text{-}I}$ mice (red) (Mann-Whitney U-test). *C1)* A sample trace. Box plots (median, interquartile range) show data from all the PCs studied. *C2)* The evoked IPSC amplitudes. *C3)* The IPSC half decay. *C4)* The IPSC rise time. *C5)* The IPSC paired-pulse (50 ms) ratio ($2^{nd}/1^{st}$ IPSC amplitude). *p* values with Mann-Whitney test.

D, The IPSCs from CCK-fibers do not show significant difference between the genotypes. *D1)* Sample trace. *D2-5)* The IPSC amplitude, IPSC half decay, the rise time and the paired-pulse ratio, respectively (Mann-Whitney test).

Figure 6. Reduced NMDAR-driven recurrent hippocampal inhibition in the NRG1$^{tg\text{-}type\text{-}I}$ mice

A, Schematic summarizes the experimental design. Optogenetic stimulation of CA1 area pyramidal cell fibers expressing ChR2 (green, CAMKII-Cre mice transfected with AAV2-ChR2-eYFP). Recurrent inhibitory IPSCs are generated by laser spot (473 nm, 3 ms) stimulation focused in *stratum pyramidale (s.p.) and oriens* (*s.o.*).

B, Sample experiments showing averaged (5) recurrent IPSCs in the CA1 pyramidal cells, evoked by the optogenetic stimulation (5 pulses at 20 Hz) in WT (*B1*) and NRG1$^{tg\text{-}type\text{-}I}$ mice (*B2*). Black traces show IPSCs in baseline, green is in the presence of NMDAR blocker DL-AP5 (100 µM, at 5-8 min after DL-AP5 application). The IPSCs were recorded at the reversal potential of EPSCs. The IPSCs were fully blocked with NBQX (25 µM, grey traces).

C, Plots show the recurrent IPSC charge in sample experiments in the WT (*C1*) and in the NRG1$^{tg\text{-}type\text{-}I}$ mouse (*C2*). Wash-in of DL-AP5 and NBQX is indicated by green and grey horizontal bars, respectively.

D, The hippocampal recurrent IPSCs in the NRG1$^{tg\text{-}type\text{-}I}$ mice show reduced sensitivity to the NMDAR antagonist. Box plot (median, interquartile range) summarizes the effect of DL-AP5 (100 µM) on the recurrent IPSC charge in the WT (blue) and the NRG1$^{tg\text{-}type\text{-}I}$ mice (red). The IPSC charge in the presence of DL-AP5 (and in the presence of NBQX) is normalized with the baseline for each experiment. *p* value with Mann-Whitney U-test.

Figure 1.

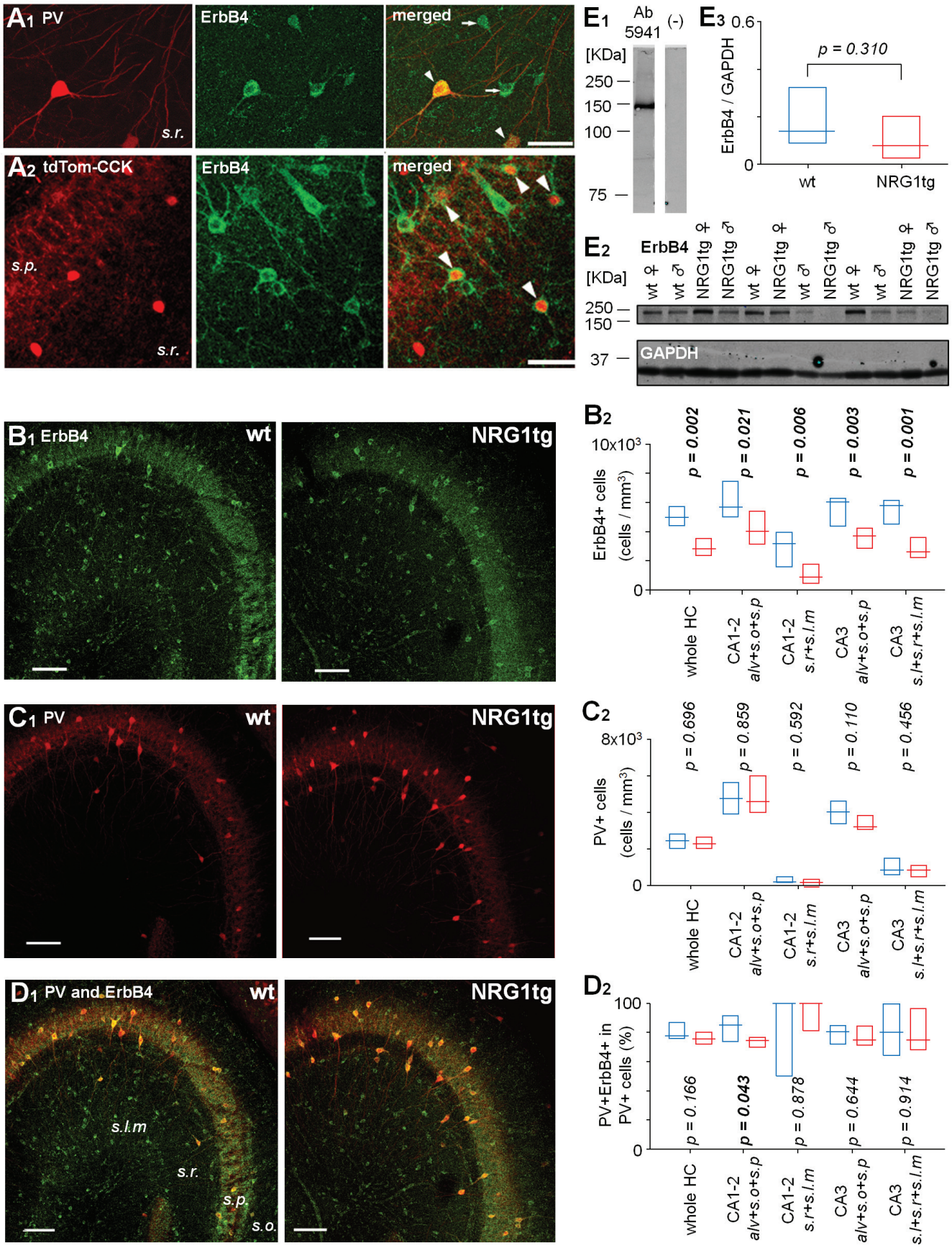

Figure 2 .

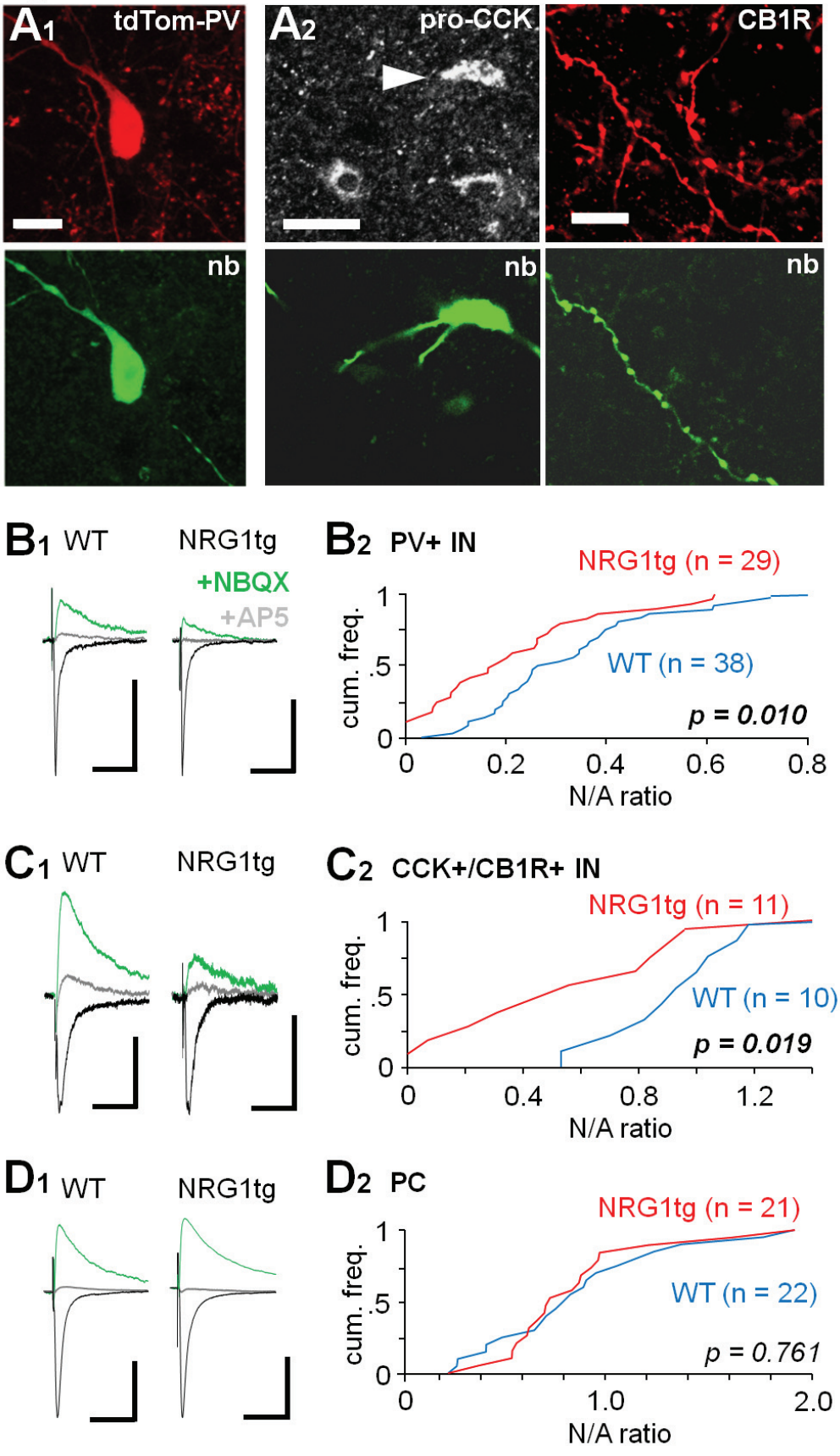

Figure 3.

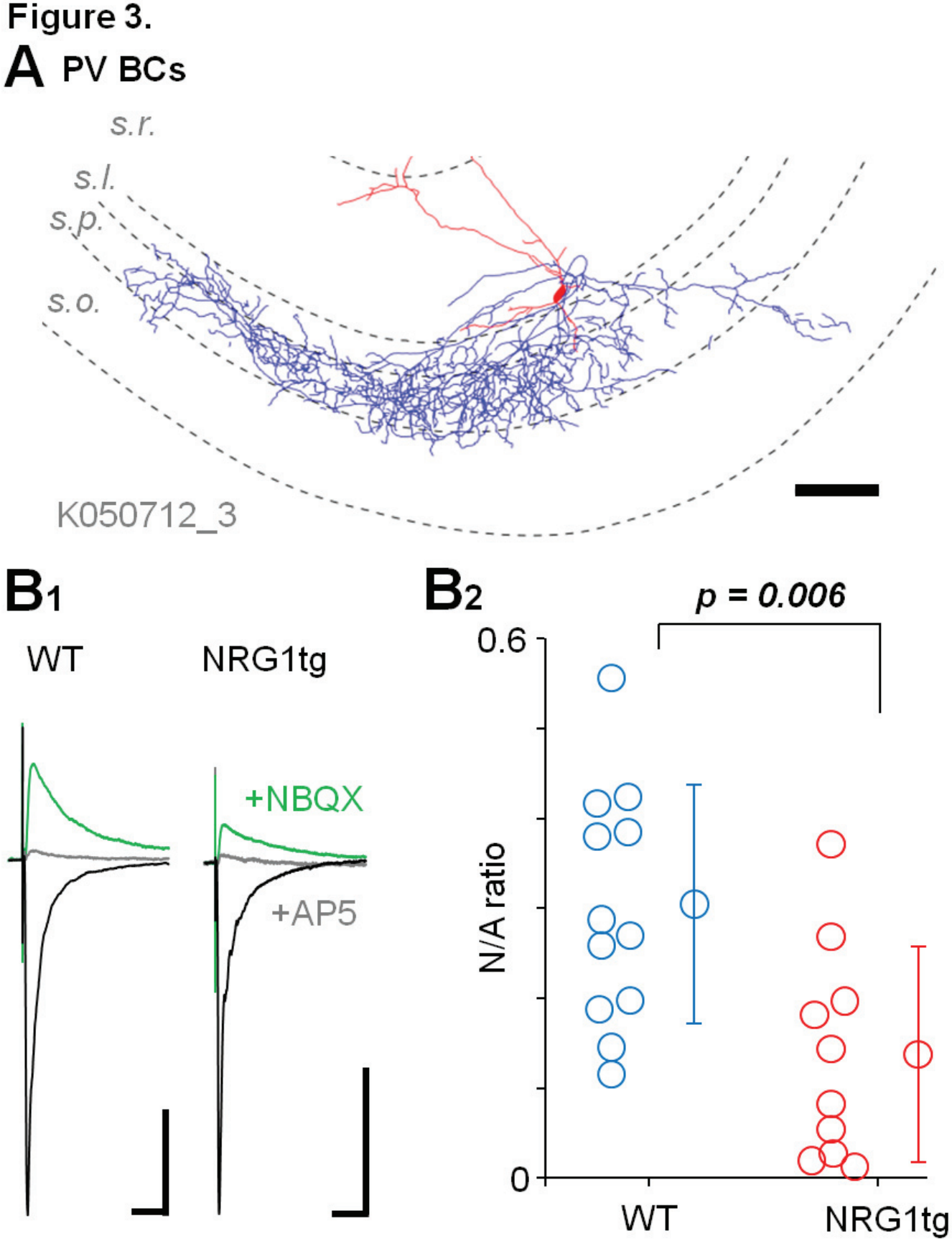

Figure 4.

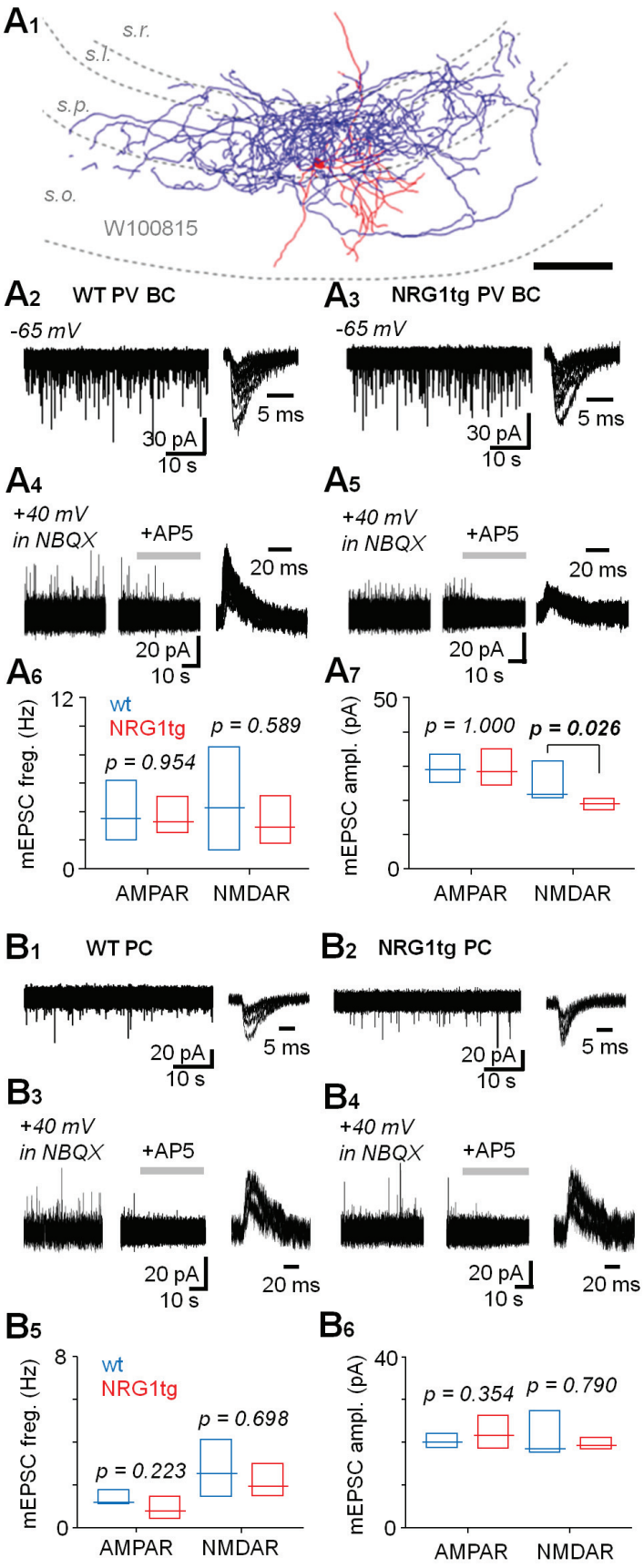

Figure 5.

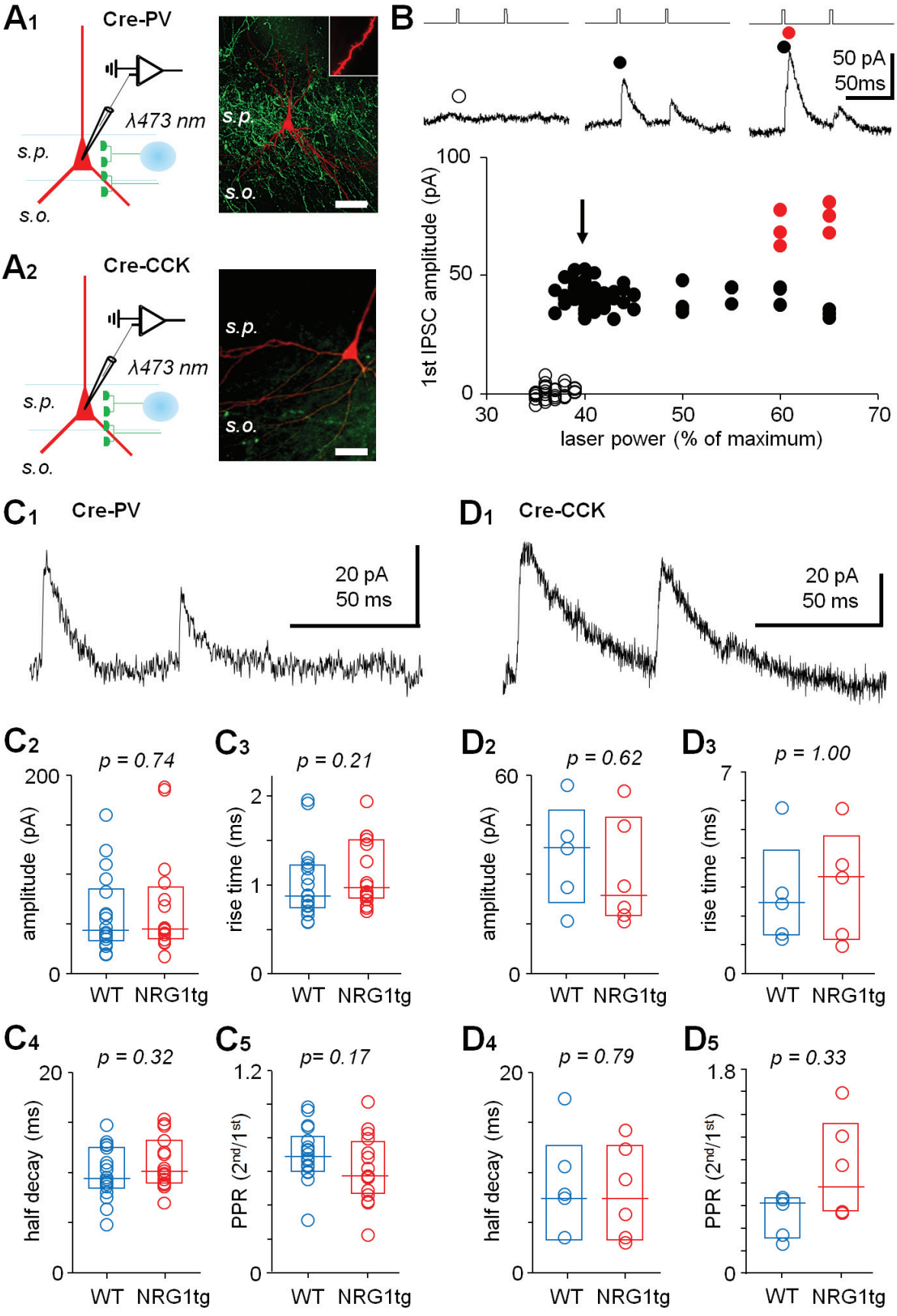

Figure 6.